PROCEEDINGS OF THE ROYAL SOCIETY A MATHEMATICAL, PHYSICAL & ENGINEERING SCIENCES

Attractor local dimensionality, nonlinear energy transfers and finite-time instabilities in unstable dynamical systems with applications to two-dimensional fluid flows

Themistoklis P. Sapsis

Proc. R. Soc. A 2013 **469**, 20120550, published 13 March 2013

PROCEEDINGS OF THE ROYAL SOCIETY A

rspa.royalsocietypublishing.org

Research

Cite this article: Sapsis TP. 2013 Attractor local dimensionality, nonlinear energy transfers and finite-time instabilities in unstable dynamical systems with applications to two-dimensional fluid flows. Proc R Soc A 469: 20120550.
http://dx.doi.org/10.1098/rspa.2012.0550

Received: 18 September 2012
Accepted: 11 February 2013

Subject Areas:
applied mathematics, complexity, fluid mechanics

Keywords:
finite-dimensional attractors, transitional flows, stochastic reduction, nonlinear dimensionality, nonlinear energy transfer, dynamical orthogonality

Author for correspondence:
Themistoklis P. Sapsis
e-mail: sapsis@mit.edu

Electronic supplementary material is available at http://dx.doi.org/10.1098/rspa.2012.0550 or via http://rspa.royalsocietypublishing.org.

Royal Society Publishing
Informing the science of the future

Attractor local dimensionality, nonlinear energy transfers and finite-time instabilities in unstable dynamical systems with applications to two-dimensional fluid flows

Themistoklis P. Sapsis

Department of Mechanical Engineering, Massachusetts Institute of Technology, 77 Massachusetts Avenue, Cambridge, MA 02139, USA

We examine the geometry of the finite-dimensional attractor associated with fluid flows described by Navier–Stokes equations and relate its nonlinear dimensionality to energy exchanges between dynamical components (modes) of the flow. Specifically, we use a stochastic framework based on the dynamically orthogonal equations to perform efficient order-reduction and describe the stochastic attractor in the reduced-order phase space in terms of the associated probability measure. We introduce the notion of local fractal dimensionality to describe the geometry of the attractor and we establish a connection with the number of positive finite-time Lyapunov exponents. Subsequently, we illustrate in specific fluid flows that the low dimensionality of the stochastic attractor is caused by the synergistic activity of linearly unstable and stable modes as well as the action of the quadratic terms. In particular, we illustrate the connection of the low-dimensionality of the attractor with the circulation of energy: (i) from the mean flow to the unstable modes (due to their linearly unstable character), (ii) from the unstable modes to the stable ones (due to a nonlinear energy transfer mechanism) and (iii) from the stable modes back to the mean (due to the linearly stable character of these modes).

1. Introduction

As Hopf first conjectured [1] for Navier–Stokes equations, it is often the case that infinite-dimensional dynamical systems posses global attractors with finite-dimensionality embedded in the infinite-dimensional state space, i.e. compact sets that attract all the trajectories of the original dynamical system. For this case, it is expected that the set of solutions that 'live' in the attractor will cover every possible realization of the original system. Conditions for the existence of such global attractors have been studied rigorously for many systems of practical importance, including the Navier–Stokes equations (see [2–5], and subsequent works by Foias and co-workers). Finite-dimensionality of these attractors implies that the asymptotic dynamics of the corresponding infinite-dimensional systems can be described by a finite number of degrees of freedom, a property that can potentially lead to efficient reduced-order modelling: a drastic decrease in the number of degrees of freedom which are essential to understand or compute the system dynamics.

Along these ideas, a number of methods have been developed for the description of the global attractor. Among them, the method of determining nodes [6] where the global attractor is represented in terms of specific points of the domain (determining nodes) that have been proved to be finite in number for the Navier–Stokes equations [7]. A different family of order-reduction methods is based on a Galerkin-type approximation [8–10], i.e. on the expansion of the solution on a finite set of basis elements and the subsequent construction of the attractor. The selection of this basis is a crucial issue for the performance of the order-reduction, and to this end, various ideas have been used such as the proper orthogonal decomposition (POD) method [11,12], which is based on energy criteria, the balanced POD method [13,14], based on linear-operator-theoretic ideas and more recently the projection to modes determined from spectral analysis of the associated Koopman operator [15].

However, in many cases of practical importance, the system response can be strongly transient. This property in combination with the time-independent character of the used modes can increase dramatically their number in order to achieve good performance, even for systems with low-dimensional attractors. Most importantly, the mean field variations are ignored while it has been shown (see recent studies [16–18]) that the mean field dynamics may be an intrinsic component of the transient character of the response. A recent methodology that can deal with the earlier-mentioned issues is based on the dynamically orthogonal (DO) field equations [19]. This is a stochastic, order-reduction approach where the modes are time-dependent, orthogonal fields computed by a set of equations that are derived rigorously from the original system equation. The evolution of these time-dependent modes is performed in a fully coupled manner with the reduced-order dynamics and the mean field dynamics. As it is discussed in detail in Sapsis & Lermusiaux [19], the main advantage of the DO method compared with other reduction methods is its ability to evolve the modes according to both the system equations and the current statistical state of the system without the use of any empirical data that describe the transient character of the response. This way the resulted set of required modes is smaller and can express more effectively the instantaneous dynamics of the full system.

The next step involves the analysis within the reduced-order phase space resulted by the projection of the dynamics on a finite number of degrees of freedom. In the reduced-order phase space of Navier–Stokes equations, there are three main contributions for the evolution of the dynamics and the formation of the global attractor, namely (i) the linearly unstable directions (associated with positive finite-time Lyapounov exponents, FTLEs) that cause expansion of volumes in phase space; (ii) the linearly stable directions (associated with negative FTLEs); and (iii) the quadratic terms (due to the nonlinear advection) that cause nonlinear deformation of volumes in phase space. As it will presented later in this work, each of those contributions can be interpreted in terms of energy transfer properties between the mean flow and the modes and between the modes themselves. *The exact scope of this study: to establish and illustrate a connection between* (*i*) *the unstable directions in the reduced-order phase space;* (*ii*) *the energy transfer properties between the evolving mean flow and the modes; and* (*iii*) *the local geometrical properties of the global attractor*.

Our theoretical findings will be illustrated numerically through fluid flows described by deterministic two-dimensional Navier–Stokes, having randomness only in the initial conditions. We will choose configurations where the system has a small number of unstable directions so that the order-reduction is an efficient method for analysis. This choice is made in order to illustrate clearly the connection between the shape of the attractor and the energy transfer properties when these are caused exclusively by inherent system instabilities (i.e. in the absence of external stochastic noise or stochastic parameters). Similar properties and conclusions, however, hold for systems with large number of instabilities although in such systems/configurations a straightforward application of order-reduction techniques may not be an efficient choice. The reduction framework that we will use here is based on the DO equations. We emphasize that even though we will use a probabilistic tool to perform our analysis, the systems under consideration will be deterministic with their unstable directions creating the finite-dimensional attractors. Essentially, we will use a stochastic approach to characterize how volumes evolve in the phase space of a deterministic dynamical system. This probabilistic point of view, even though it will be applied on a deterministic system, it will allow us to characterize the geometrical properties of the attractor that are otherwise hard to capture through a 'single-trajectory' approach especially when the system is in a transient stage.

The structure of the paper is organized as follows. We first give a brief overview of the DO method as an order-reduction technique and we also present comparison results (see the electronic supplementary material, appendix S1) between the DO method and a standard POD approach for two two-dimensional fluid flows. Next, we introduce the notion of local fractal dimensionality to describe the geometry of the global attractor. Based on this tool, we prove the main result which is a link between (i) the energy transfer properties (expressed through the modal productions (see [20] or [16]), i.e. the energy transfer rates to a specific mode from the mean and/or other modes, (ii) the associated finite time Lyapunov exponents (FTLE) and (iii) the local geometry of the attractor. We illustrate the derived theorem in the Lorenz attractor, and subsequently, we proceed to the application on the responses of two-dimensional Navier–Stokes equations for two specific configurations. Through these examples, we illustrate how the synergistic activity of linearly stable and unstable modes together with the action of the quadratic nonlinearities cause energy transfers from the mean to and between the modes, while simultaneously it creates the complex geometry of the attractor.

2. Order-reduction, using dynamical orthogonality

Our analysis is based on the dynamically orthogonal field equations [19,21]. This is a closed set of equations for the evolution of stochastic partial differential equations (SPDEs) based on the dynamical orthogonality condition, a constraint that arises naturally to overcome the unnecessary redundancy of the used representation. The DO framework allows for the evolution of the probability measure through exact equations that follow directly from the SPDE associated with the considered problem and without any assumption on its form (e.g. assumption of a particular distribution for the uncertainty or a specific spatial structure). Specifically, the reduced-order field equations allow for the simultaneous (i) evolution of the finite-dimensional functional space where the stochastic part of the solution 'lives' (i.e. the spatio-temporal form of the modes) and (ii) description of the system dynamics within this finite-dimensional functional space.

This ensemble framework allows for the statistical study of the attractor and its geometrical properties in the reduced-order subspace even for transient flows. The system under consideration is chosen to be deterministic, and only the initial conditions are chosen to be random variables. However, this randomness in the initial conditions is sufficient to obtain a statistical picture of the attractor. In particular, *the attractor will be expressed as the subset of the reduced-order space where the probability measure associated with the stochastic solution has non-zero values*, i.e. the finite-dimensional subset where solutions of the PDE converge with non-zero probability. We will use the ordinary differential equation (ODE) governing the reduced-order

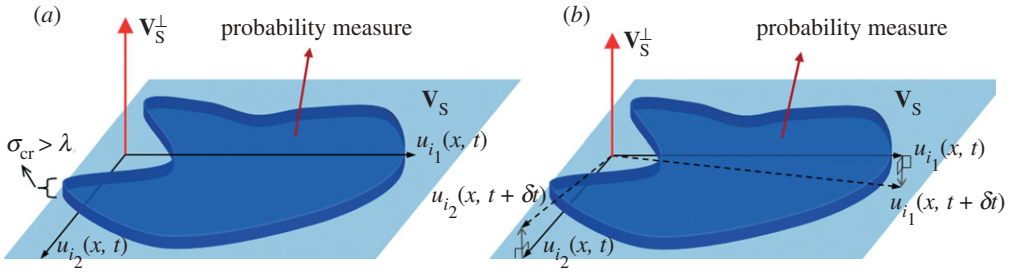

Figure 1. (*a*) Partition of the infinite-dimensional space into a finite-dimensional subspace $\mathbf{V}_S$ containing only the directions u_i along which the probability measure of the solution has important spread (greater than λ) and its orthogonal complement $\mathbf{V}_S^\perp$. (*b*) The variation of each basis element should be normal to the subspace $\mathbf{V}_S$. (Online version in colour.)

dynamics to interpret the local geometry of the attractor in terms of energy transfers between the mean and the stochastic parts of the flow.

Here, we give a brief description of the dynamical orthogonality condition that allows for the derivation of closed field equations governing both the reduced-order dynamics and the finite-dimensional subspace $\mathbf{V}_S$ where these dynamics 'live'. A comparison with POD method on two specific flows has been included in the electronic supplementary material, appendix S1. Let $(\Omega, \mathcal{B}, \mathcal{P})$ be a probability space with Ω being the sample space containing the set of elementary events $\omega \in \Omega$, $\mathcal{B}$ is the $\sigma-$algebra associated with Ω and $\mathcal{P}$ is a probability measure. Let $x \in D \subseteq \mathbb{R}^n$ denote the spatial variables and $t \in T$ the time. Then, every measurable map of the form $u(x, t; \omega) \in \mathbb{R}^n, \omega \in \Omega$ will define a random field. In applications, the most important cases are where $n = 2, 3$, therefore we will assume that $x \in D \subseteq \mathbb{R}^n$, $n = 2, 3$. We define the mean value operator as

$$\bar{u}(x, t) = E^\omega[u(x, t; \omega)] = \int_\Omega u(x, t; \omega)\, \mathrm{d}\mathcal{P}(\omega).$$

A Hilbert space denoted by $\mathbf{H}$, is formed by the set of all continuous, square-integrable random fields [22,23], i.e. $\int_D E^\omega[u(x, t; \omega)u(x, t; \omega)^{\mathrm{T}}]\, \mathrm{d}x < \infty$ for all $t \in T$ (where $\bullet^{\mathrm{T}}$ denotes the complex conjugate operation). We also define the covariance operator

$$\mathbf{C}_{u_1(\cdot,t;\omega)u_2(\cdot,s;\omega)}(x, y) = E^\omega[(u_1(x, t; \omega) - \bar{u}_1(x, t))(u_2(y, s; \omega) - \bar{u}_2(y, s))^{\mathrm{T}}] \tag{2.1}$$

For every two elements $u_1, u_2 \in \mathbf{H}$, we denote the spatial inner product as $\langle u_1(\bullet, t; \omega), u_2(\bullet, t; \omega)\rangle$. In what follows, we will use Einstein's convention for summation, i.e. $\sum_i a_i b_i = a_i b_i$ except if the limits of summation need to be shown.

Using a generalized form (each term is time-dependent and we do not assume Gaussian statistics) of the Karhunen–Loeve expansion [19], we have that every random field $u(x, t; \omega) \in \mathbf{H}$ can be approximated arbitrarily well, by a finite series of the form

$$u(x, t; \omega) = \bar{u}(x, t) + \sum_{i=1}^{s} Y_i(t; \omega) u_i(x, t), \quad \omega \in \Omega, \tag{2.2}$$

where s is a sufficiently large, non-negative integer and the $Y_i(t; \omega)$ are s scalar random coefficients. We define the stochastic subspace $\mathbf{V}_S = \mathrm{span}\{u_i(x, t)\}_{i=1}^s$ as the linear space spanned by the s deterministic fields $u_i(x, t)$. This subspace includes the finite number of directions (of the full infinite-dimensional space) where the probability measure has important spread, i.e. larger than a predefined value λ (figure 1*a*). The orthogonal complement of $\mathbf{V}_S$ contains the infinite number of dimensions associated with low-variance dynamics, i.e. the directions of the infinite-dimensional phase space where the probability measure have negligible variance.

Clearly, representation (2.2) with all quantities $(\bar{u}(x, t), \{u_j(x, t)\}_{j=1}^s, \{Y_j(t; \omega)\}_{j=1}^s)$ varying is redundant, and, therefore, additional constraints are need to be imposed so that we have a numerically well-posed problem. As shown in Sapsis & Lermusiaux [19], an appropriate

constraint is the DO condition: the variation of the stochastic subspace (figure 1*b*) should always remain orthogonal to itself, expressed as

$$\frac{\mathrm{d}\mathbf{V}_S}{\mathrm{d}t} \perp \mathbf{V}_S \;\Leftrightarrow\; \left\langle \frac{\partial u_i(\bullet,t)}{\partial t}, u_j(\bullet,t) \right\rangle = 0, \quad i=1,\ldots,s,\;\; j=1,\ldots,s. \tag{2.3}$$

Note that the DO condition implies the preservation of orthonormality for the basis $\{u_j(x,t)\}_{j=1}^{s}$ itself because $(\partial/\partial t)\langle u_i(\bullet,t), u_j(\bullet,t)\rangle = 0$ for all $i=1,\ldots,s, j=1,\ldots,s$. The DO expansion results in a set of independent, explicit equations for all the unknown quantities. In particular, using the DO expansion, we reformulate the system SPDE to an s-dimensional stochastic differential equation for the random coefficients $Y_i(t;\omega)$ coupled with $s+1$ deterministic PDEs for the fields $\bar{u}(x,t)$ and $u_i(x,t)$. In particular, we have the following.

Theorem 2.1 (Sapsis & Lermusiaux [19]). *Let the SPDE be*

$$\frac{\partial u(x,t;\omega)}{\partial t} = \mathcal{L}[u(x,t;\omega);\omega], \quad x\in D,\;\; t\in T,\;\; \omega\in\Omega, \tag{2.4}$$

where $\mathcal{L}$ is a general (nonlinear), differential operator. Additionally, we assume that the initial state of the system at t_0 is described by the random field $u(x,t_0;\omega)=u_0(x;\omega)$, $x\in D$, $\omega\in\Omega$, and the boundary conditions are given by $\mathcal{B}[u(\xi,t;\omega)]=h(\xi,t;\omega), \xi\in\partial D, \omega\in\Omega$. Under the assumptions of the DO representation, the original SPDE (2.4) is reduced to the following system of equations

$$\frac{\mathrm{d}Y_i(t;\omega)}{\mathrm{d}t} = \langle \mathcal{L}[u(\bullet,t;\omega);\omega] - E^{\omega}[\mathcal{L}[u(\bullet,t;\omega);\omega]], u_i(\bullet,t)\rangle, \tag{2.5}$$

$$\frac{\partial \bar{u}(x,t)}{\partial t} = E^{\omega}[\mathcal{L}[u(x,t;\omega);\omega]] \tag{2.6}$$

and

$$\frac{\partial u_i(x,t)}{\partial t} = \boldsymbol{\Pi}_{\mathbf{V}_S^{\perp}}[E^{\omega}[\mathcal{L}[u(x,t;\omega);\omega]Y_j(t;\omega)]]\mathbf{C}^{-1}_{Y_i(t)Y_j(t)}, \tag{2.7}$$

where the projection in the orthogonal complement of the stochastic subspace is defined as $\boldsymbol{\Pi}_{\mathbf{V}_S^{\perp}}[F(x)] = F(x) - \boldsymbol{\Pi}_{\mathbf{V}_S}[F(x)] = F(x) - \langle F(\bullet), u_k(\bullet,t)\rangle u_k(x,t)$ and the covariance coefficients $\mathbf{C}_{Y_i(t)Y_j(t)} = E^{\omega}[Y_i(t;\omega)Y_j(t;\omega)]$. The associated boundary conditions have the form

$$\mathcal{B}[\bar{u}(\xi,t;\omega)]|_{\xi\in\partial D} = E^{\omega}[h(\xi,t;\omega)]$$

and

$$\mathcal{B}[u_i(\xi,t)]|_{\xi\in\partial D} = E^{\omega}[Y_j(t;\omega)h(\xi,t;\omega)]\mathbf{C}^{-1}_{Y_i(t)Y_j(t)},$$

and the initial conditions are given by

$$Y_i(t_0;\omega) = \langle u_0(\bullet;\omega) - \bar{u}(x,t_0), \upsilon_i(\bullet)\rangle, \quad \bar{u}(x,t_0) = E^{\omega}[u_0(x;\omega)], \quad u_i(x,t_0) = \upsilon_i(x),$$

for all $i=1,\ldots,s$, where $\upsilon_i(x)$ are the eigenfields of the covariance operator $\mathbf{C}_{u(\cdot,t_0)u(\cdot,t_0)}$.

3. Local fractal dimensionality of the attractor

Here, we present the tools that we use later to study the geometry of the finite-dimensional attractor. These stochastic tools do not assume anything on the form of the attractor neither on the dimensionality of the support where the attractor 'lives'. Specifically, our analysis is based on the interplay between the attractor as the subset where the probability density function of the system state is finite (or important), and the attractor as a continuous collection of points whose Lagrangian properties define its evolution and its local geometrical properties. The connection between the two interpretations will be introduced through a suitable definition of the fractal dimensionality of the local support of the attractor, i.e. the neighbourhood at each point of the attractor where the probability measure (associated with the attractor) has non-negligible spread.

The set-up is defined by the reduced-order dynamics in the stochastic subspace $\mathbf{V}_S$ (see §2 for definition) that can be fully described by the finite-dimensional, dynamical system (equation (2.5))

$$\frac{\mathrm{d}Y_i}{\mathrm{d}t} = F_i(\mathbf{Y}, t), \quad \mathbf{Y}(t_0; \omega) = \mathbf{Y}_0(\omega), \quad \mathbf{Y} \in \mathbb{R}^s, \tag{3.1}$$

where $F_i(\mathbf{Y}, t)$ is a smooth, deterministic, dynamical system that comes directly from the projection of the dynamics to the DO modes. We denote as $P_{\mathbf{Y}}$ the probability measure associated with the state of the dynamical system (3.1) and as $f_Y(\mathbf{y}, t)$ the corresponding probability density function. Note that, in this work, we consider the case where uncertainty is introduced only through the initial conditions and not through the system operator—from this assumption, it follows that F_i is deterministic.

We will first present standard expressions for the stretching of infinitesimal lengths under the influence of the dynamical system (3.1). Subsequently, we will use these expressions to explore the mechanism for the instantaneous decrease in the dimensionality associated with the local support of the probability measure at each point of the phase space. Specifically, we will prove that the mechanism causing collapse of the probability measure to lower dimensional manifolds (or in the general case attractors) is connected with the negative eigenvalues of the variational flow associated with the dynamical system (3.1). In §3*b*, we will use the notion of the Cauchy–Green tensor to generalize these conclusions over finite-time intervals. To this end, we will provide a connection between the local dimensionality of the support of the probability measure and the number of positive FTLEs (see Haller [24] for their definition).

Let us first recall some standard expressions for the stretching of infinitesimal lengths in the time-varying stochastic subspace $\mathbf{V}_S$. We consider the variational equation associated with (3.1) given by $\mathrm{d}(\delta Y_i)/\mathrm{d}t = (\partial F_i(\mathbf{Y}, t)/\partial Y_j)\delta Y_j$. Then, the length l of an infinitesimal vector having direction described by the unitary vector $\mathbf{n}$, i.e. a vector with components $\delta Y_i = n_i l$ will be given by $l^2 = \delta Y_i \delta Y_i$. Therefore,

$$l\frac{\mathrm{d}l}{\mathrm{d}t} = \frac{\mathrm{d}(\delta Y_i)}{\mathrm{d}t}\delta Y_i = \delta Y_i \frac{\partial F_i(\mathbf{Y}, t)}{\partial Y_j}\delta Y_j = l^2 \frac{\partial F_i(\mathbf{Y}, t)}{\partial Y_j} n_i n_j = l^2 \mathbf{n}^{\mathrm{T}} D_Y \mathbf{F} \mathbf{n}, \tag{3.2}$$

where $D_Y\mathbf{F} = (\boldsymbol{\nabla}_{\mathbf{Y}}\mathbf{F}(\mathbf{Y}, t) + [\boldsymbol{\nabla}_{\mathbf{Y}}\mathbf{F}(\mathbf{Y}, t)]^{\mathrm{T}})/2$. The above scalar quantity expresses the stretching of an infinitesimal length, with orientation defined by the normal vector $\mathbf{n}$, owing to the dynamical flow in the reduced-order phase space.

(a) Evolution of the support of the probability measure dimensionality over infinitesimal times

The next step of our analysis involves the evolution of the local dimensionality of the support of the probability measure $P_{\mathbf{Y}}$ associated with the dynamical system (3.1). In the absence of stochastic forcing in equation (3.1), the probability density f_Y corresponding to the measure $P_{\mathbf{Y}}$ is evolving according to the Liouville's equation [25, p. 200]

$$\frac{\partial f_Y}{\partial t} + \frac{\partial [F_i(\mathbf{y}, t) f_Y]}{\partial y_i} = 0.$$

The linearity of the evolution operator also holds for the case where we have stochastic forcing with white noise characteristics (or in general any independent increment process; [25]) but also for the general case of stochastic forcing [26]. To this end, it is meaningful to study the evolution of the dimensionality locally in the phase space, i.e. for just an ε-small segment of the probability measure because each of those segments of probability evolve independently. Therefore, we partition the probability measure $P_{\mathbf{Y}}$ into ε-small segments $P_{\varepsilon,i}$ with centres $\mathbf{y}_i$ (so that $f_Y(\mathbf{y}, t) = \sum_i f_{\varepsilon,i}(\mathbf{y}, t)$) and we study those independently from each other (figure 2). We assume that ε is chosen to be sufficiently small so that each of the probability measures $P_{\varepsilon,i}$ can be approximated as uniform over the sphere $S_\varepsilon(\mathbf{y}_i) = \{\mathbf{x} \in \mathbf{V}_S : \|\mathbf{x} - \mathbf{y}_i\| < \varepsilon\}$ and only along the directions over which the original probability measure $P_{\mathbf{Y}}$ has spread of probability.

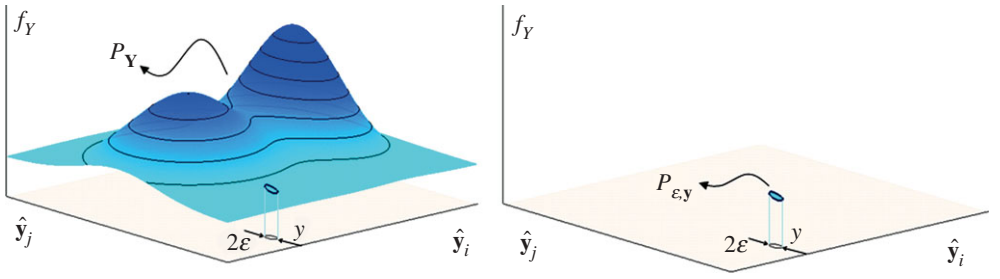

Figure 2. (*a*,*b*) Splitting of the probability density function in 'smaller' probability measures having a sufficiently small support of diameter ε so that the probability density can be approximated as uniform. (Online version in colour.)

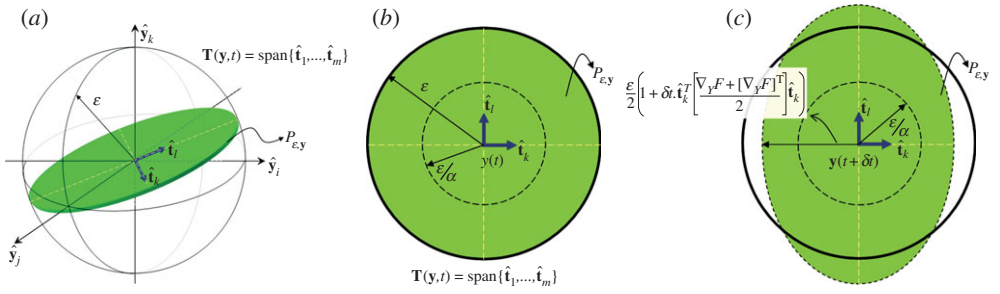

Figure 3. (*a*) Uniform probability measure $P_{\varepsilon,\mathbf{y}}$ with support on the intersection of the space $\mathbf{T}(\mathbf{y},t) = \mathrm{span}\{\hat{\mathbf{t}}_1,\ldots,\hat{\mathbf{t}}_m\}$ and the sphere $S_\varepsilon(\mathbf{y})$. (*b*,*c*) Evolution of the probability measure $P_{\varepsilon,\mathbf{y}}$ over an infinitesimal time. The volume that remains inside the sphere $S_\varepsilon(\mathbf{y})$ is studied by examining the length of the principal axes (dashed lines). (Online version in colour.)

In order to define the local dimensionality of the support of the probability measure $P_{\mathbf{Y}}$ around each trajectory $\mathbf{y}(t) \in \mathbf{V}_S$, we consider the closest ε-small segment $P_{\varepsilon,i}$ that we denote from here on as $P_{\varepsilon,\mathbf{y}}$ and we define its dimensionality as $\vartheta(\mathbf{y},t) = \lim_{\varepsilon\to 0} \log V_P[\mathbf{y}(t),\varepsilon]/\log\varepsilon$, where $V_P[\mathbf{y}(t),\varepsilon]$ is the volume of the points $\mathbf{x}$ (i.e. integral of the Lebesque measure) that lie inside the sphere $S_\varepsilon(\mathbf{y}(t)) = \{\mathbf{x}\in\mathbf{V}_S : \|\mathbf{x}-\mathbf{y}(t)\| < \varepsilon\}$ and over which the probability measure $P_{\varepsilon,\mathbf{y}}$ is non-zero (see Pesin [27] for a complete discussion of its properties). For technical reasons, we will use a variant of the above expression which comes from the fact that both the numerator and the denominator vanish as $\varepsilon \to 0$. Then, from l'Hôpital's rule, we have the equivalent definition

$$\vartheta(\mathbf{y},t) = \lim_{\varepsilon\to 0} \frac{\log V_P[\mathbf{y}(t),\varepsilon] - \log V_P[\mathbf{y}(t),\varepsilon/\alpha]}{\log\varepsilon - \log(\varepsilon/\alpha)}, \tag{3.3}$$

where α is an arbitrary positive number which without loss of generality is chosen to be $\alpha > 1$. While the previous definition gives an absolute measure for the dimensionality of the support of the probability measure $P_{\varepsilon,\mathbf{y}}$, this latter definition gives this dimensionality relatively, i.e. by examining the volume between the two spheres $S_\varepsilon(\mathbf{y})$ and $S_{\varepsilon/\alpha}(\mathbf{y})$. *This definition gives an effective measure of dimensionality that can change over finite times under the effect of smooth dynamics. This is not the case for the absolute dimensionality of a smooth measure that will remain invariant over finite times under the effect of smooth dynamics.*

Before we study of the evolution of these volumes, i.e. $S_\varepsilon(\mathbf{y})$ and $S_{\varepsilon/\alpha}(\mathbf{y})$, we first give a characterization of a uniform probability measure that lives in the sphere $S_\varepsilon(\mathbf{y}(t))$ and has dimensionality $m \le s$. Because we have a uniform measure, we need only the tangent bundle $\mathbf{T}(\mathbf{y},t) = \mathrm{span}\{\mathbf{t}_1,\ldots,\mathbf{t}_m\}$ (where $\dim\mathbf{T}(\mathbf{y},t) = m$) of the manifold where it lives i.e. we need the basis vectors describing the directions over which the probability measure $P_{\varepsilon,\mathbf{y}}$ has non-zero spread (figure 3*a*).

Then, we restrict our analysis along the directions only in $\mathbf{T}(\mathbf{y},t)$, because over all the other directions the 'thickness' of the probability measure is zero, and according to (3.2), it will remain zero (because the distance of any points lying in the support of $P_{\varepsilon,\mathbf{y}}$ along these directions is zero).

To determine the volume change in $V_P[\mathbf{y}(t),\varepsilon]$ along the trajectory $\mathbf{y}(t)$, we will study the length change in each of the principal axis (dashed lines in figure 3*b*,*c*). This will be given according to formula (3.2) as

$$l_k(t+\delta t) = l_k(t)(1+\delta t.\mathbf{t}_k^{\mathrm{T}} D_Y\mathbf{F}.\mathbf{t}_k), \quad k=1,\ldots,m.$$

The change in $V_P[\mathbf{y}(t),\varepsilon]$ over time will only be caused by the directions $\mathbf{t}_k$ over which we have reduction of lengths, i.e. the directions for which $\mathbf{t}_k^{\mathrm{T}}[(\boldsymbol{\nabla}_{\mathbf{Y}}\mathbf{F}(t,\mathbf{Y}) + [\boldsymbol{\nabla}_{\mathbf{Y}}\mathbf{F}(t,\mathbf{Y})]^{\mathrm{T}})/2]\mathbf{t}_k < 0$ because $V_P[\mathbf{y}(t+\delta t),\varepsilon]$ measures only the volume of the support of $P_{\varepsilon,\mathbf{y}}$ that remains inside the sphere $\|\mathbf{x}-\mathbf{y}(t+\delta t)\| < \varepsilon$. Therefore, we will have

$$\frac{V_P[\mathbf{y}(t+\delta t),\varepsilon]}{V_P[\mathbf{y}(t),\varepsilon]} = 1 + \delta t \sum_{\substack{k=1,\ldots,m \\ \mathbf{t}_k^{\mathrm{T}} D_Y\mathbf{F}.\mathbf{t}_k<0}} \mathbf{t}_k^{\mathrm{T}} D_Y\mathbf{F}.\mathbf{t}_k + \mathcal{O}(\delta t^2). \tag{3.4}$$

Moreover, α can always be chosen sufficiently large so that $V_P[\mathbf{y}(t+\delta t),\varepsilon/a] = V_P[\mathbf{y}(t),\varepsilon/a]$. With this choice and by combining (3.3) and (3.4), we obtain the instantaneous rate of change for the local dimensionality of the probability measure

$$\frac{\mathrm{d}\vartheta(\mathbf{y},t)}{\mathrm{d}t} = \frac{1}{\log\alpha} \sum_{\substack{k=1,\ldots,m \\ \mathbf{t}_k^{\mathrm{T}} D_Y\mathbf{F}.\mathbf{t}_k<0}} \mathbf{t}_k^{\mathrm{T}} D_Y\mathbf{F}.\mathbf{t}_k \leq 0. \tag{3.5}$$

A first observation for equation (3.5) is the absence of a specific time scale over which the variation of the dimensionality of the ε-probability measure takes place. This is due to the fact that we chose the quantity α arbitrarily. The characteristic time scale over which the probability measure will change dimensionality depends on the volume size that we are examining and in this case this is the volume between the spheres $S_\varepsilon(\mathbf{y})$ and $S_{\varepsilon/\alpha}(\mathbf{y})$. The closer these two spheres are (i.e. $\alpha \to 1^+$), the faster the change in the dimensionality will occur ($\mathrm{d}\vartheta(\mathbf{y},t)/\mathrm{d}t \to -\infty$). Similarly, the larger this volume is (i.e. $\alpha \to \infty$), the slower the change in the dimensionality will take place ($\mathrm{d}\vartheta(\mathbf{y},t)/\mathrm{d}t \to 0^-$).

We emphasize that the result (3.5) is local in space and time, and it cannot be used to determine the dimensionality variation of the support of the probability measure along a trajectory over a finite time interval because we have made the assumption that at time t the probability measure $P_{\varepsilon,\mathbf{y}}$ covers uniformly all the directions of $\mathbf{T}(\mathbf{y},t)$ in the complete extend of the sphere $S_\varepsilon(\mathbf{y}) = \{\mathbf{x} \in \mathbf{V}_S : \|\mathbf{x}-\mathbf{y}\| < \varepsilon\}$; therefore, *the growth of the dimensionality cannot be expressed in this setting*. From a technical point of view, this simplification is allowed from the fact that at every time instant we choose (or more precisely restart our analysis with) an arbitrarily small sphere $S_\varepsilon(\mathbf{y})$ to perform the above argument. However, if we fix an initial radius ε and study the dimensionality of the probability measure along a finite interval of a trajectory (in this case, we cannot 'renew' the ε-probability measure at every time instant), then we may initially have temporal decrease in the dimensionality owing to shrinking of the probability measure over a specific direction but then subsequent increase because in this particular direction that so far we had reduction of lengths we now have extension of lengths. This finite-time behaviour will be considered in §3*b*.

Therefore, formula (3.5) expresses the *maximum possible decrease* in the dimensionality of the support of the probability measure on every time instant and phase space location. This expression can be used to understand under what conditions the dimensionality of the support of the probability measure will stop decreasing. This will occur if and only if the tangent bundle of the support of the probability measure becomes normal to the negative subspace of $D_Y\mathbf{F}(\mathbf{y},t)$, i.e. the subspace spanned by the eigenvectors of $D_Y\mathbf{F}(\mathbf{y},t)$ that correspond to negative eigenvalues. Therefore, *the low dimensionality of the support of the probability measure is caused by the negative eigenvalues of the tensor* $D_Y\mathbf{F}(\mathbf{y},t)$. More specifically, the local dimensionality of the support of the probability measure at $(\mathbf{y},t)$ will not stop vary unless it becomes smaller or equal to the

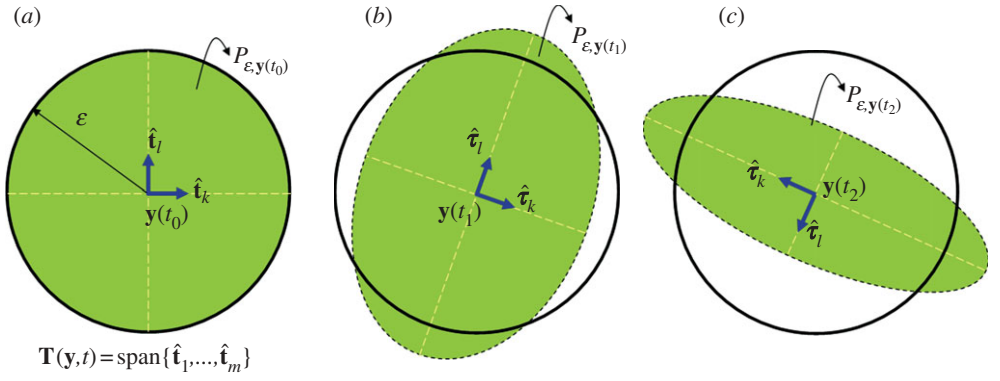

Figure 4. Evolution of the probability measure $P_{\varepsilon,\mathbf{y}}$ over a finite time interval. Note that each $\hat{\boldsymbol{\tau}}_i$ does not necessarily express the evolution of $\hat{\mathbf{t}}_i$ but one of the principal directions of the evolved ellipsoid. From t_0 to t_1, we have contraction along the principal axis $\hat{\boldsymbol{\tau}}_k$. However, over the second time interval (t_1, t_2), we have much stronger expansion over this direction (which also evolves under the dynamical flow). (Online version in colour.)

number of positive eigenvalues of $D_Y\mathbf{F}(\mathbf{y},t)$. Moreover, it is required that the low dimensional probability measure is aligned with the positive subspace $D_Y\mathbf{F}(\mathbf{y},t)$, i.e. the subspace spanned by the eigenvectors of $D_Y\mathbf{F}(\mathbf{y},t)$ that corresponds to positive eigenvalues.

(b) Evolution of the probability measure dimensionality over finite times

In §3*a*, we illustrated how the presence of negative eigenvalues in the symmetric tensor $D_Y\mathbf{F}(\mathbf{y},t)$ is the underlying cause for dimensionality reduction of the support of the probability measure $P_{\varepsilon,\mathbf{y}}$. However, as we emphasized, the analysis was based on the setting that the probability measure under consideration is at every time instant t uniformly distributed in the intersection of the linear space $\mathbf{T}(\mathbf{y},t)$ and the interior of the sphere $S_\varepsilon(\mathbf{y})$. In this way, we did not allow for expansion of the dimensionality of the support of the probability measure. This assumption was made to understand the dynamical cause of low dimensionality. In this section, we will analyse how the probability measure dimensionality varies along a trajectory owing to the combined effect of instantaneous stretching (because of the negative eigenvalues in $D_Y\mathbf{F}(\mathbf{y},t)$ as explained before) but also transport under the flow (3.1) that causes rotation of the low-dimensional support of $P_{\varepsilon,\mathbf{y}}$ and may lead to temporal contraction over a specific direction and subsequent expansion over the same direction (figure 4).

To quantify the variation of the dimensionality over a finite time interval, we consider the flow map $\varphi_{t_0}^t$ that maps any point $\mathbf{y}_0$ in $\mathbf{V}_S$ to its position at time t under the effect of the dynamical system (3.1)

$$\boldsymbol{\varphi}_{t_0}^t : \mathbf{V}_S \to \mathbf{V}_S, \quad \mathbf{y}_0 \mapsto \mathbf{y}(t, t_0, \mathbf{y}_0).$$

Then, the evolution along the above trajectory of any infinitesimally small vector $\boldsymbol{\nu}$ will be given by $\boldsymbol{\nabla}\boldsymbol{\varphi}_{t_0}^t\boldsymbol{\nu}$. Moreover, its corresponding length $l_{\boldsymbol{\nu}}(t)$ will be given by

$$l_{\boldsymbol{\nu}}^2(t) = \boldsymbol{\nu}^{\mathrm{T}}[\boldsymbol{\nabla}\boldsymbol{\varphi}_{t_0}^t]^{\mathrm{T}}\boldsymbol{\nabla}\boldsymbol{\varphi}_{t_0}^t\boldsymbol{\nu} = \boldsymbol{\nu}^{\mathrm{T}}C_{t_0}^t(\mathbf{y}_0)\boldsymbol{\nu},$$

where $C_{t_0}^t(\mathbf{y}_0) = [\boldsymbol{\nabla}\boldsymbol{\varphi}_{t_0}^t(\mathbf{y}_0)]^{\mathrm{T}}\boldsymbol{\nabla}\boldsymbol{\varphi}_{t_0}^t(\mathbf{y}_0)$ is the Cauchy–Green tensor [28] which is by definition symmetric and positive-definite. We diagonalize $C_{t_0}^t(\mathbf{y}_0)$ to obtain a set of real, positive, eigenvalues

$$0 < \lambda_1^2(\mathbf{y}_0, t_0, t) \le \lambda_2^2(\mathbf{y}_0, t_0, t) \le \cdots \le \lambda_s^2(\mathbf{y}_0, t_0, t)$$

with corresponding eigenvectors $\hat{\mathbf{e}}_j(\mathbf{y}_0, t_0, t)$, $j = 1, \ldots, s$. The directions given by these eigenvectors describe the directions of principal deformation. By inverting the variational flow,

we may obtain the initial directions $\hat{\boldsymbol{\epsilon}}_j(\mathbf{y}_0, t_0, t)$ associated with these eigenvectors. These will be given by (in normalized form)

$$\hat{\boldsymbol{\epsilon}}_j(\mathbf{y}_0, t_0, t) = \lambda_j(\mathbf{y}_0, t_0, t)[\boldsymbol{\nabla}\boldsymbol{\varphi}_{t_0}^t]^{-1}\hat{\mathbf{e}}_j(\mathbf{y}_0, t_0, t) = \lambda_j(\mathbf{y}_0, t_0, t)\boldsymbol{\nabla}\boldsymbol{\varphi}_t^{t_0}\hat{\mathbf{e}}_j(\mathbf{y}_0, t_0, t).$$

Note that even though the above set of vectors always span the s-dimensional space, they are not necessarily orthogonal (because the matrix $\boldsymbol{\nabla}\boldsymbol{\varphi}_{t_0}^t$ is invertible but not necessarily orthogonal).

Then, we define the following subspaces that separate the initial directions over which we have expansion of lengths at time t from those over which we have contraction

$$\mathbf{T}^e(\mathbf{y}_0, t_0, t) = \mathrm{span}\{\hat{\boldsymbol{\epsilon}}_j(\mathbf{y}_0, t_0, t) \mid \lambda_j(\mathbf{y}_0, t_0, t) \geq 1\}$$

and

$$\mathbf{T}^c(\mathbf{y}_0, t_0, t) = \mathrm{span}\{\hat{\boldsymbol{\epsilon}}_j(\mathbf{y}_0, t_0, t) \mid \lambda_j(\mathbf{y}_0, t_0, t) < 1\}.$$

These two subspaces span the full s-dimensional space and they are also orthogonal. The first property follows from the fact that the flow $\boldsymbol{\varphi}_{t_0}^t$ has been assumed to be invertible and the eigenvectors $\hat{\mathbf{e}}_j(\mathbf{y}_0, t_0, t)$, $j = 1, \ldots, s$ span the full space. The second property can be proved by assuming that there is a vector $\mathbf{r}_0$ that belongs both to $\mathbf{T}^e$ and $\mathbf{T}^c$. Then, because $\mathbf{r}_0 \in \mathbf{T}^e$, i.e. $\mathbf{r}_0 = \sum_{j=1}^{\dim \mathbf{T}^e} a_j\hat{\boldsymbol{\epsilon}}_j(\mathbf{y}_0, t_0, t)$ (with a_j scalars) the evolution of the length under the variational flow will be expressed as

$$\begin{aligned} l_{\mathbf{r}_0}^2(t) &= \mathbf{r}_0^{\mathrm{T}} C_{t_0}^t(\mathbf{y}_0)\mathbf{r}_0 \\ &= \sum_{j,k} a_j a_k \lambda_j(\mathbf{y}_0, t_0, t)\lambda_k(\mathbf{y}_0, t_0, t)\hat{\mathbf{e}}_j^{\mathrm{T}}(\mathbf{y}_0, t_0, t)[\boldsymbol{\nabla}\boldsymbol{\varphi}_t^{t_0}]^{\mathrm{T}} C_{t_0}^t(\mathbf{y}_0)\boldsymbol{\nabla}\boldsymbol{\varphi}_t^{t_0}\hat{\mathbf{e}}_k(\mathbf{y}_0, t_0, t) \\ &= \sum_{j,k} a_j a_k \lambda_j(\mathbf{y}_0, t_0, t)\lambda_k(\mathbf{y}_0, t_0, t)\hat{\mathbf{e}}_j^{\mathrm{T}}(\mathbf{y}_0, t_0, t)\hat{\mathbf{e}}_k(\mathbf{y}_0, t_0, t) \\ &= a_j^2\lambda_j^2(\mathbf{y}_0, t_0, t) \geq a_j a_j = l_{\mathbf{r}_0}^2(t_0), \end{aligned}$$

where in the above we used the fact that $\boldsymbol{\nabla}\boldsymbol{\varphi}_t^{t_0}\boldsymbol{\nabla}\boldsymbol{\varphi}_{t_0}^t = \mathbf{I}$ as well as the orthonormality of $\hat{\mathbf{e}}_j(\mathbf{y}_0, t_0, t)$ (which follows from the properties of $C_{t_0}^t(\mathbf{y}_0)$). Because $\mathbf{r}_0 \in \mathbf{T}^c$, we may use the same argument to prove that $l_{\mathbf{r}_0}^2(t) < l_{\mathbf{r}_0}^2(t_0)$ which contradicts the previous result. Therefore, $\mathbf{T}^e(\mathbf{y}_0, t_0, t) \oplus \mathbf{T}^c(\mathbf{y}_0, t_0, t) = \mathbf{V}_{\mathrm{S}}$.

In order to study the variation of the dimensionality of the support of the probability measure, we use the same setting as previously, i.e. we consider an ε-probability measure uniformly distributed on the intersection of the sphere interior $S_\varepsilon(\mathbf{y}_0)$ and the linear subspace $\mathbf{T}(\mathbf{y}_0, t_0) = \mathrm{span}\{\mathbf{t}_1, \ldots, \mathbf{t}_m\}$ (with $\dim \mathbf{T}(\mathbf{y}_0, t_0) = m$), which represents the directions over which the probability measure has initial spread. To compute the principal directions of the evolved ellipsoid, we need to diagonalize the Cauchy–Green tensor within the subspace $\mathbf{T}(\mathbf{y}_0, t_0)$, i.e. solve a restricted eigenvalue problem in the subspace $\mathbf{T}(\mathbf{y}_0, t_0)$:

$$C_{t_0}^t(\mathbf{y}_0)\boldsymbol{\tau} = \eta^2\boldsymbol{\tau}, \quad \boldsymbol{\tau} \in \boldsymbol{T}(\mathbf{y}_0, t_0).$$

We express the arbitrary element $\boldsymbol{\tau} \in \mathbf{T}(\mathbf{y}_0, t_0)$ as $\boldsymbol{\tau} = \sum_{i=1}^m a_i\mathbf{t}_i$ and we define the $s \times m$ matrix $\mathcal{T} = [\mathbf{t}_1, \mathbf{t}_2, \ldots, \mathbf{t}_m]$. Then, the above eigenvalue problem can be expressed equivalently as the regular eigenvalue problem

$$\mathcal{T}^{\mathrm{T}} C_{t_0}^t(\mathbf{y}_0)\mathcal{T}\mathbf{a} = \eta^2\mathbf{a}, \quad \mathbf{a} \in \mathbb{R}^m.$$

The $m \times m$ matrix of this eigenvalue problem is symmetric and positive-definite. Therefore, we can always determine the principal directions of the ellipsoid as well as their length that will be given by the eigenvalues

$$0 < \eta_1^2(\mathbf{y}_0, t_0, t) \leq \eta_2^2(\mathbf{y}_0, t_0, t) \leq \cdots \leq \eta_m^2(\mathbf{y}_0, t_0, t).$$

Then, the volume of the support of the probability measure $P_{\varepsilon,\mathbf{y}_0}$ at time t that will remain inside the sphere $S_\varepsilon(\boldsymbol{\varphi}_{t_0}^t(\mathbf{y}_0))$ will be given by $V_{P,\varepsilon}|_t = \varepsilon^m \prod_{j=1}^m \min(\eta_j(\mathbf{y}_0, t_0, t), 1)$ and the corresponding

dimensionality as

$$\vartheta(\mathbf{y}, t) = m + \lim_{\varepsilon \to 0} \frac{1}{\log \varepsilon} \sum_{j=1}^{m} \log \min(\eta_j(\mathbf{y}_0, t_0, t), 1) \leq m. \tag{3.6}$$

Now, let us separate the conditions under which we have constant dimensionality from those where we have decrease in the dimensionality. We will have decrease in the dimensionality if and only if there is at least one eigenvalue $\eta_j(\mathbf{y}_0, t_0, t) < 1$. This is equivalent with the minimum condition

$$\min_{\mathbf{a} \in \mathbb{R}^m} \mathbf{a}^{\mathrm{T}} \mathcal{T}^{\mathrm{T}} C_{t_0}^{t}(\mathbf{y}_0) \mathcal{T} \mathbf{a} < 1 \;\Leftrightarrow\; \min_{\boldsymbol{\tau} \in \mathbf{T}(\mathbf{y}_0, t_0)} \boldsymbol{\tau}^{\mathrm{T}} C_{t_0}^{t}(\mathbf{y}_0) \boldsymbol{\tau} < 1.$$

The second condition will occur if and only if $\mathbf{T}(\mathbf{y}_0, t_0)$ contains a direction that is included in $\mathbf{T}^c(\mathbf{y}_0, t_0, t)$. On the other hand, if $\mathbf{T}(\mathbf{y}_0, t_0)$ is a subset of the expansion eigenspace $\mathbf{T}^e(\mathbf{y}_0, t_0, t)$ then

$$\min_{\boldsymbol{\tau} \in \mathbf{T}(\mathbf{y}_0, t_0)} \boldsymbol{\tau}^{\mathrm{T}} C_{t_0}^{t}(\mathbf{y}_0) \boldsymbol{\tau} > 1 \;\Leftrightarrow\; \min_{\mathbf{a} \in \mathbb{R}^m} \mathbf{a}^{\mathrm{T}} \mathcal{T}^{\mathrm{T}} C_{t_0}^{t}(\mathbf{y}_0) \mathcal{T} \mathbf{a} > 1 \;\Leftrightarrow\; \min_{j=1,\ldots,m} \eta_j(\mathbf{y}_0, t_0, t) > 1.$$

and the dimensionality will not change. Therefore, the dimensionality of the support of the probability measure $P_{\varepsilon, \mathbf{y}_0}$ will remain invariant over the time interval (t_0, t) if and only if

$$\mathbf{T}(\mathbf{y}_0, t_0) \subseteq \mathbf{T}^e(\mathbf{y}_0, t_0, t), \tag{3.7}$$

i.e. the probability measure is locally distributed only along directions that correspond to expansion. On the other hand, if the probability measure has spread over a direction over which we have contraction the dimensionality of its support will decrease according to formula (3.6).

From (3.7), we immediately obtain the necessary condition

$$\dim \mathbf{T}(\mathbf{y}_0, t_0) \leq \dim \mathbf{T}^e(\mathbf{y}_0, t_0, t).$$

Therefore, the local dimensionality of the probability measure cannot exceed at any point $\mathbf{y}$ the number of positive eigenvalues of the Cauchy–Green tensor $C_{t_0}^{t}(\mathbf{y}_0)$ (also called forward FTLEs; see Haller [24]), otherwise, its dimensionality will decrease over the specified time interval. Applying the above analysis on every point in the support of $P_{\mathbf{y}}$ leads to theorem 3.1.

Theorem 3.1. *The dimensionality of the support of the probability measure $P_{\mathbf{y}}$ will remain invariant over the time interval (t_0, t) if and only if at every point $\mathbf{y} \in \mathbf{V}_S$ the support of the probability measure $\mathbf{T}(\mathbf{y}, t_0)$ (i.e. the directions over which the probability measure has spread) is a subset of the corresponding expansion subspace $\mathbf{T}^e(\mathbf{y}, t_0, t)$.*

Thus, for a probability measure having initial spread in every direction in $\mathbf{V}_S$ the dimensionality of its support will continue to decrease until it has been aligned at every point in phase space with the expansion eigenspace $\mathbf{T}^e$ of the Cauchy–Green tensor. We emphasize that the above analysis does not exclude the possibility of a probability measure having a support with variable local dimensionality over the space $\mathbf{V}_S$. In fact, such probability measures will be presented in the section that follows and which is related to fluid flows. The above analysis gives a geometrical description of the probability measure associated with the general dynamical system (3.1).

Example (dimensionality of the Lorenz attractor). For dissipative dynamical systems with chaotic behaviour, a connection between the properties of the attractor and the Lyapunov exponents of the system is given by the theory of SRB measures (see Young [29] for a survey). In this example, the goal is to illustrate the connection between the number of positive FTLE and the global fractal dimensionality of the attractor. We are interested to establish this connection with FTLE because this is the appropriate tool to handle instabilities in systems with strong

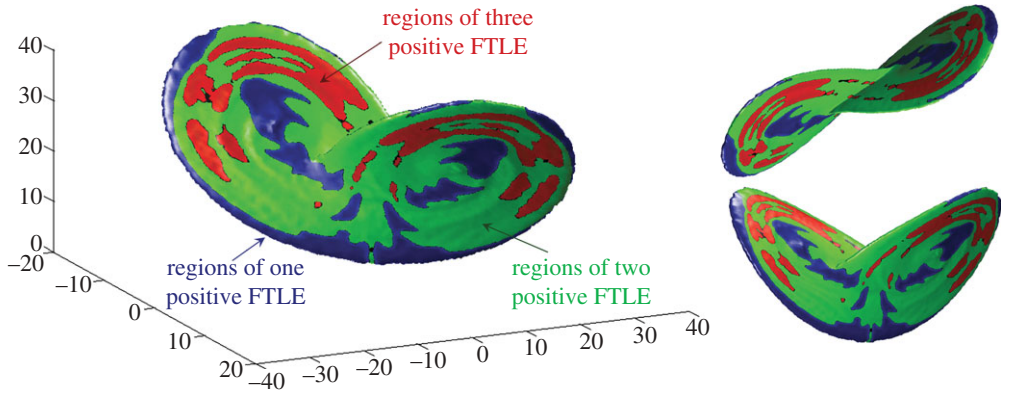

Figure 5. Lorenz attractor: a low contour ($f_Y = 10^{-6}$) of the probability density function shaded according to the number of positive FTLE. Arrows in the graph show regions of a single, two and three positive FTLE. (Online version in colour.)

time-dependence (as those that we will describe in the next sections). We consider the Lorenz equations [30]

$$\frac{dY_1}{dt} = \sigma(Y_2 - Y_1), \quad \frac{dY_2}{dt} = Y_1(\rho - Y_3) - Y_2, \quad \frac{dY_3}{dt} = Y_1 Y_2 - \beta Y_3,$$

with parameter values $\sigma = 10$, $\beta = \frac{8}{3}$ and $\rho = 28$. For this set of parameters, the system exhibits chaotic behaviour, and the attractor has no absolute continuity a property that leads to a fractal dimensionality between 2 and 3 [31]. This is a global measure of the attractor dimensionality, i.e. it is an averaged indicator over the support of the attractor, and here we seek to interpret this result in terms of the local number of positive FTLE using the conclusions of the previous sections.

We integrate a large set of initial conditions for $\delta t_{\mathrm{INTEG}} = 4$ and we plot the probability density function of the system state (computed using a high-resolution histogram). This is shown through a low contour $\{(Y_1, Y_2, Y_3) \,|\, f_Y = 10^{-6}\}$ in figure 5—the colouring is according to the number of positive FTLE which are computed over a finite-time interval $\delta t_{\mathrm{FTLE}} = 1.6$ as the eigenvalues of the Cauchy–Green tensor (for details on the computation of the FTLE, we refer to [32,33]). Specifically, dark (blue) regions indicate domains of a single positive FTLE, light regions (green), domains with two positive FTLE and grey regions (red in online version) domains with three positive FTLE. Then, in accordance with the previous discussion, the segments of the probability measure that pass over each region will tend to acquire a support with dimensionality specified by the number of the positive FTLE. From figure 5, we observe that the majority of the attractor is characterized by two positive FTLE, whereas there are some regions in the main body of the attractor with three positive FTLE. Finally, the blue regions (one positive FTLE) are mainly localized in the edges of the attractor and have much lower effect on the global dimensionality because the residence time of the system trajectories over this regions is much smaller compared with the other domains. Thus, the main part of the probability measure resides in regions with two positive FTLE consistently with the correlation dimension of the attractor that is found to be 2.05 ± 0.01 [31].

We note that the above analysis does not provide with a global measure of fractal dimensionality but rather with a local, in time and phase space, measure of 'effective' dimensionality that follows from a statistical perspective (because it is based on many realizations) and yet it reflects properties of individual realizations such as dynamical instabilities. This kind of local analysis does not contradict with global, fractal measures of dimensionality (such as the Kaplan–Yorke dimension, the correlation dimension and others), when those exist, but it illustrates how these can form as a result of an attractor along which there are different regions of dynamical behaviour.

4. Geometry of the attractor and finite-time instabilities in fluid flows

In this section, we focus on specific properties of the reduced-order dynamics associated with fluid flows described by Navier–Stokes. In particular, we study how geometrical properties of the attractor in the reduced-order phase space vary in terms of energy transfer properties in the original infinite-dimensional space (such as energy transfer between DO modes and the mean). As mentioned in §1, we consider the case of a homogeneous system, i.e. no external stochastic forcing or stochastic boundary conditions. Specifically, we consider an incompressible, three-dimensional fluid in a domain D, described in a rotating frame at frequency f with dynamical equations

$$\frac{\partial \mathbf{u}}{\partial t} = -\boldsymbol{\nabla} p + \frac{1}{Re}\Delta \mathbf{u} - \mathbf{u}.\boldsymbol{\nabla}\mathbf{u} - f\hat{\mathbf{k}} \times \mathbf{u} + \boldsymbol{\tau}(\mathbf{x}, t) \equiv \mathcal{L}_{\mathbf{u}}[\mathbf{u}(\mathbf{x}, t; \omega)]$$

and

$$0 = \operatorname{div} \mathbf{u},$$

where $\mathbf{u} = (u_1(\mathbf{x}, t; \omega), u_2(\mathbf{x}, t; \omega), u_3(\mathbf{x}, t; \omega))$ is the flow velocity field, and $\hat{k}$ is the unit vector in the z-direction. The pressure field is denoted by $p(\mathbf{x}, t; \omega)$, $f = f_0 + \beta_0 y$ is the Coriolis coefficient under the beta plane approximation, and $\boldsymbol{\tau}(\mathbf{x}, t) = (\tau_1(\mathbf{x}, t), \tau_2(\mathbf{x}, t), \tau_3(\mathbf{x}, t))$ is the external deterministic stress acting on the fluid. In what follows, we will use the DO field equations with inner product $\langle \mathbf{u}_1, \mathbf{u}_2 \rangle = \int_D u_{1i} u_{2i}\, \mathrm{d}\mathbf{x}$. We assume that the boundary conditions for the flow field and the pressure are described by the linear differential operators: $\mathcal{B}_{\mathbf{u}}[\mathbf{u}(\boldsymbol{\xi}, t; \omega)] = \mathbf{u}_{\partial D}(\boldsymbol{\xi}, t)$, $\mathcal{B}_p[p(\boldsymbol{\xi}, t; \omega)] = p_{\partial D}(\boldsymbol{\xi}, t)$, $\boldsymbol{\xi} \in \partial D$, and we also have the initial conditions: $\mathbf{u}(\mathbf{x}, t_0; \omega) = \mathbf{u}_0(\mathbf{x}; \omega)$, $\mathbf{x} \in D$, $\omega \in \Omega$. In this case, as it is illustrated in Sapsis & Lermusiaux [19], the dynamical system describing the stochastic flow in the reduced-order space $\mathbf{V}_S$ takes the form (equation (2.5))

$$\frac{\mathrm{d}Y_i}{\mathrm{d}t} = A_{im}(t) Y_m + B_{imn}(t) Y_m Y_n + D_i, \tag{4.1}$$

where

$$A_{im} = \left\langle \frac{1}{Re}\Delta \mathbf{u}_m - \mathbf{u}_m.\boldsymbol{\nabla}\bar{\mathbf{u}} - \bar{\mathbf{u}}.\boldsymbol{\nabla}\mathbf{u}_m - f\hat{\mathbf{k}} \times \mathbf{u}_m, \mathbf{u}_i \right\rangle,$$

$$B_{imn} = -\langle \mathbf{u}_n.\boldsymbol{\nabla}\mathbf{u}_m, \mathbf{u}_i \rangle$$

and

$$D_i = \mathbf{C}_{Y_m(t)Y_n(t)} \langle \mathbf{u}_n.\boldsymbol{\nabla}\mathbf{u}_m, \mathbf{u}_i \rangle.$$

Therefore, for fluids governed by Navier–Stokes equations the reduced-order dynamics are described, as expected, by a nonlinear dynamical system, with time-dependent coefficients that has quadratic nonlinearities.

To understand the geometrical properties of the solutions of this dynamical system, we study the deformation (across different directions) of infinitesimal volumes in $\mathbf{V}_S$ as well as the evolution of the dimensionality of these volumes using the tools developed in the previous sections. We begin our analysis by proving an important symmetry property for the tensor B_{imn} that follows from Greens identity and the orthonormality of the modes:

Lemma 4.1. *Assume that the incompressible modes* $\mathbf{u}_i$ *are orthonormal. Then, the tensor* $B_{imn} = -\langle \mathbf{u}_n.\boldsymbol{\nabla}\boldsymbol{u}_m, \mathbf{u}_i \rangle$ *satisfies the following antisymmetry condition*

$$B_{imn} = -B_{\mathrm{min}}. \tag{4.2}$$

Proof. See electronic supplementary material, appendix S2. ■

The next step of our analysis involves the study of the infinitesimal volumes in the reduced-order space $\mathbf{V}_S$. We first compute the Jacobian

$$\frac{\partial F_i}{\partial Y_k} = A_{ik}(t) + (B_{ikn}(t) + B_{ink}(t)) Y_n.$$

Then, we compute the change in an infinitesimal volume $V(t)$ along a trajectory $Y(t;\omega)$. By Liouville's theorem, the volume $V(t)$ satisfies

$$V(t) = V(t_0)\exp\left\{\int_{t_0}^{t} A_{kk}(t) + B_{knk}(t)Y_n|_{\mathbf{Y}=\mathbf{Y}(s;\omega)}\,\mathrm{d}s\right\},$$

where we have used the antisymmetry property (4.2) which results in $B_{kkn}(t) = 0$.

To understand the physical meaning of the terms involved in the last expression, we compute

$$A_{kk} = \left\langle \frac{1}{Re}\Delta\mathbf{u}_k - \mathbf{u}_k.\boldsymbol{\nabla}\bar{\mathbf{u}} - \bar{\mathbf{u}}.\boldsymbol{\nabla}\mathbf{u}_k - f\hat{\mathbf{k}}\times\mathbf{u}_k, \mathbf{u}_k\right\rangle.$$

The Coriolis contribution is skew symmetric, thus, $(f\hat{\mathbf{k}}\times\mathbf{u}_k)\mathbf{u}_k = 0 \Rightarrow \langle f\hat{\mathbf{k}}\times\mathbf{u}_k, \mathbf{u}_k\rangle = 0$. Moreover, from the Gauss theorem

$$\langle\bar{\mathbf{u}}.\boldsymbol{\nabla}\mathbf{u}_k, \mathbf{u}_k\rangle = \frac{1}{2}\int_D u_{k,i}u_{k,i}\frac{\partial\bar{u}_j}{\partial x_j}\,\mathrm{d}\mathbf{x} + \frac{3}{2}\int_{\partial D} u_{k,i}u_{k,i}\bar{u}_j n_j\,\mathrm{d}s.$$

The first term on the right-hand side vanishes because $\partial\bar{u}_j/\partial x_j = 0$, and the boundary integral also vanishes as we proved in the proof of the antisymmetry property for the tensor B_{inm}. Additionally,

$$\langle\mathbf{u}_k.\boldsymbol{\nabla}\bar{\mathbf{u}}, \mathbf{u}_k\rangle = \int_D \frac{\partial\bar{u}_i}{\partial x_j}u_{k,j}u_{k,i}\,\mathrm{d}\mathbf{x} = \int_D \frac{1}{2}\left(\frac{\partial\bar{u}_i}{\partial x_j} + \frac{\partial\bar{u}_j}{\partial x_i}\right)u_{k,j}u_{k,i}\,\mathrm{d}\mathbf{x} = \langle\mathbf{u}_k\mathbf{S}_{\bar{\mathbf{u}}}, \mathbf{u}_k\rangle,$$

where $\mathbf{S}_{\mathbf{u}}$ is the strain tensor for the flow field $\mathbf{u}$. Therefore,

$$A_{kk} = -\frac{1}{Re}\sum_{k=1}^{s}\|\boldsymbol{\nabla}\mathbf{u}_k\|^2 - \langle\mathbf{u}_k\mathbf{S}_{\bar{\mathbf{u}}}, \mathbf{u}_k\rangle.$$

Moreover,

$$B_{knk}Y_n = -\langle\mathbf{u}_k.\boldsymbol{\nabla}\mathbf{u}_n, \mathbf{u}_k\rangle Y_n = -\langle\mathbf{u}_k.\boldsymbol{\nabla}\mathbf{u}_n, \mathbf{u}_k\rangle Y_n = -\langle\mathbf{u}_k.\mathbf{S}_{\mathbf{u}}, \mathbf{u}_k\rangle + \langle\mathbf{u}_k.\mathbf{S}_{\bar{\mathbf{u}}}, \mathbf{u}_k\rangle.$$

Thus, we have

$$\begin{aligned}\frac{V(t)}{V(t_0)} &= \exp\left\{\int_{t_0}^{t}\left(-\frac{1}{Re}\sum_{k=1}^{s}\|\boldsymbol{\nabla}\mathbf{u}_k\|^2 - \langle\mathbf{u}_k\mathbf{S}_{\mathbf{u}}, \mathbf{u}_k\rangle\right)\mathrm{d}s\right\}\\ &= \exp\left\{\int_{t_0}^{t}\left(-\frac{1}{Re}\sum_{k=1}^{s}\|\boldsymbol{\nabla}\mathbf{u}_k\|^2 - \langle\mathbf{u}_k\mathbf{S}_{\bar{\mathbf{u}}}, \mathbf{u}_k\rangle\right)\mathrm{d}s - \int_{t_0}^{t}\langle\mathbf{u}_k.\boldsymbol{\nabla}\mathbf{u}_n, \mathbf{u}_k\rangle Y_n(s)\,\mathrm{d}s\right\}. \qquad (4.3)\end{aligned}$$

Equation (4.3) expresses the expansion of the probability measure along a trajectory of the dynamical system (4.1) in the reduced-order stochastic subspace $\mathbf{V}_S$. This change in infinitesimal volumes is due to:

— viscous dissipation term, $-(1/Re)\|\boldsymbol{\nabla}\mathbf{u}_k\|^2$, which is always causing contraction of volumes in the phase space and it has a *uniform effect* over the whole space $\mathbf{V}_S$;
— energy exchanged between the DO modes and the mean flow, $-\langle\mathbf{u}_k\mathbf{S}_{\bar{\mathbf{u}}}, \mathbf{u}_k\rangle$, which can cause both contraction and expansion of volumes and it is *uniform* in phase space; and
— energy exchanged between the DO modes, $-\langle\mathbf{u}_k.\boldsymbol{\nabla}\mathbf{u}_n, \mathbf{u}_k\rangle Y_n$ which cause transfer of volumes within the stochastic subspace and it is non-uniform.

The first two terms, i.e. dissipation owing to viscosity and energy exchange with the mean flow, do not change the probability of occurrence in the 'neighbourhood' of any specific trajectory $Y(t;\omega)$ relative to another one, because the effect of these mechanisms is homogeneous (their effect does not depend on the specific position of the trajectory $Y(t;\omega)$) over the whole space $\mathbf{V}_S$ or over all trajectories $Y(t;\omega)$. The effect of these terms is the uniform increase or decrease in the support of the probability measure, i.e. the increase or decrease in the range of possible stochastic realizations because, due to these terms, the probability density spreads to a wider range into the stochastic subspace $\mathbf{V}_S$. This spread occurs uniformly along each direction y_i (defined by the

basis elements $\mathbf{u}_i$) of the stochastic subspace $\mathbf{V}_S$ but it is not necessarily identical over different directions of the stochastic subspace.

To give a more quantitative illustration, we consider a more formal notion for the spread of the probability measure given by the energy $\mathcal{E}_\mathbf{Y} = \int_{\mathbf{V}_S} \|\mathbf{y}\|^2 f_\mathbf{Y}(\mathbf{y}, t)\, \mathrm{d}\mathbf{y}$. We have directly from the system equations

$$Y_i \frac{\mathrm{d}Y_i}{\mathrm{d}t} = A_{im}(t) Y_i Y_m + B_{imn}(t) Y_i Y_m Y_n + D_i Y_i.$$

The term $B_{imn}(t) Y_i Y_m Y_n$ vanishes from the antisymmetric property of B_{imn}. Therefore, we will have

$$\frac{1}{2} \frac{\mathrm{d}\mathcal{E}_\mathbf{Y}}{\mathrm{d}t} = \sum_{i=1}^{s} \left(-\frac{1}{Re} \|\boldsymbol{\nabla} \mathbf{u}_i\|^2 - \langle \mathbf{u}_i \mathbf{S}_{\bar{\boldsymbol{u}}}, \mathbf{u}_i \rangle \right) E^\omega[Y_i^2], \tag{4.4}$$

which is another manifestation of the property that we described previously, i.e. that the size of the support of the probability measure is changing solely due to the energy production due to the mean flow (i.e. the energy transfers to or from the mean flow) and due to the energy dissipation caused by the viscosity. Pressure does not play a role for this equation (describing energy of the modes) because the stochastic boundary conditions are homogeneous—this is not the case for the mean flow energy equation which will, in general, contain terms involving pressure.

On the other hand, the term $B_{imn}(t)$, *which expresses interaction among the DO modes and causes transfers of energy among them, does not cause global change in the probability measure support size* (as it is shown from (4.4)) *but it causes, however, local change in its shape* and strong deformation in the phase space owing to the non-homogeneous effect around each trajectory $Y(t;\omega)$ (see equation (4.3)). In fact, this term plays a key role because it transfers energy from the linearly unstable modes to the linearly stable ones, allowing the former to remain unstable while their energy does not explode, and the latter to always have non-zero energy while they retain their stable character.

The combined effect of the linear instabilities and this quadratic term can be quantified through the FTLEs of the reduced-order system. Specifically, directions in $\mathbf{T}^e(\mathbf{y}_0, t_0, t)$, i.e. directions that correspond to positive FTLEs, tend to increase their energy (or variance) as time evolves (because lengths are increasing along these directions). In the context of the reduced-order dynamics, this occurs owing to the combined effect of energy transfer from the mean flow (as explained previously), energy exchanges with other DO modes (caused by the quadratic term), and energy loss owing to viscous dissipation.

On the other hand, directions that correspond to negative Lyapunov exponents (belonging in $\mathbf{T}^c(\mathbf{y}_0, t_0, t)$) will tend to decrease lengths (therefore the variance) along these directions, because they lose energy from the interaction with the mean flow, the other DO modes, and through viscous dissipation as well. This flow of energy from the mean field, to the DO modes, and then back to the mean field again and its consequences on the dimensionality of the support of the probability measure associated with the attractor will become more evident in §5 where numerical results will illustrate clearly this mechanism.

5. Attractors in fluid flows with random initial conditions

Here, we will validate the theoretical results presented previously in unstable fluid flows described by deterministic equations and with random initial conditions. The reduced-order dynamics will be resolved using the DO method. The specific details for resolving Navier–Stokes equations in the framework of DO equations can be found in Sapsis *et al*. [34] while the description of the numerical scheme used in this paper is given in Ueckermann *et al*. [35]. We will compute the time-dependent modes and subsequently we will illustrate numerically in the reduced-order phase space the relation between the geometrical properties of the probability measure of the response, the local number of finite-time dynamical instabilities, as well as the energy transfers.

This connection will be shown through the computation at each point of the stochastic subspace $\mathbf{V}_S$, of (i) the number of positive, forward, FTLEs and (ii) the energy production (or energy transfer rates) of each DO mode owing to the mean flow but also owing to the other

DO modes. These two dynamical indicators of the system instabilities will be directly compared with the local dimensionality of the support of the probability measure. The latter will be shown through three-dimensional marginals that will be visualized using very low contour surfaces that contain the main probability mass.

The FTLE field will be computed using the reduced-order dynamical system (4.1) which is deterministic (because the randomness comes only from the initial conditions and not from the system operator) and known at every time instant from the DO stochastic solution. Specifically, a set of initial conditions is placed on a uniform grid and is advected under the dynamical flow (4.1) with a fourth-order Runge–Kutta solver (see Lekien *et al*. [33] for details on FTLE in multi-dimensional systems). The grid of initial conditions covers only regions of the stochastic subspace $\mathbf{V}_S$ where the probability measure has non-zero values for computational efficiency. This procedure allows to compute the Cauchy–Green tensor whose eigenvalues give the number of positive FTLE at each location where the probability measure has non-zero values.

The modal energy productions owing to the mean flow and the various DO modes will be computed using exact expressions that can be derived for the case of Navier–Stokes equations. Specifically, for each mode i, we will have the rate of energy dissipation, the energy production owing to the mean flow, and the energy production owing to all the other modes given by (see [21], §5*e* or [34])

$$\left.\begin{aligned} &\mathcal{D}_i = -E^{\omega}[Y_i^2]\frac{\|\boldsymbol{\nabla}\mathbf{u}_i\|^2}{Re}, \quad \mathcal{P}_{\text{mean}\to i} = -E^{\omega}[Y_i^2]\int_D \mathbf{u}_i^{\mathrm{T}}\mathbf{S}_{\bar{\mathbf{u}}}\mathbf{u}_i\,\mathrm{d}\mathbf{x} \\ \text{and} \quad &\mathcal{P}_{\text{DO}\to i} = E^{\omega}[Y_i Y_p Y_q]\int_D \mathbf{u}_q^{\mathrm{T}}\mathbf{S}_{\mathbf{u}_i}\mathbf{u}_p\,\mathrm{d}\mathbf{x}. \end{aligned}\right\} \tag{5.1}$$

To understand the energy flow among different spatial scales, we will define a spatio-temporal-averaged wavenumber for each DO mode. The exact definition of this averaged spatial wavenumber follows from the homogeneous spectral theory and is defined as the ratio between enstrophy and energy of each mode. Because the DO modes are normalized, their energy will be equal to one. Therefore,

$$\bar{k}_i^2 = \frac{1}{T}\int_0^T\int \|\boldsymbol{\nabla}\times\mathbf{u}_i\|^2\,\mathrm{d}\mathbf{x}\,\mathrm{d}t. \tag{5.2}$$

The flows that we will study are those that we use for the comparison with the POD method (electronic supplementary material, appendix S1): the flow behind the cylinder for $Re = 100$ and the double gyre flow with deterministic excitation for $Re = 35$. Both flows will be initiated with random initial conditions having very small stochastic energy and we will focus on the transient dynamical regime.

(a) Flow behind a cylinder

We consider the flow behind a cylinder in the instability regime for $Re = 100$. The details for this particular flow in the context of DO equations (initial conditions, number and form of modes, global energy transfers, etc) can be found in Sapsis *et al*. [34]. As soon as the symmetric wake starts to develop, the flow becomes unstable and the variance of the first antisymmetric mode starts to grow. During this uncertainty growth, new modes are adaptively added, all of them having coefficients with normal distribution and very small variance (10^{-6}). During this initial period, the statistics of the flow remain Gaussian.

After the energy of the modes becomes important enough, we have interaction with the mean flow leading to a strongly non-Gaussian, symmetric, probability measure that is localized over a two-dimensional manifold. This can be seen in figure 6 where we present the mean flow together with the first four DO modes (out of the eight used when the flow has been fully developed), in terms of the vorticity field, at three different time instants, as well as a visualization of the probability density function through the contours $\{(Y_1, Y_2, Y_3)\,|\,f_{Y_1Y_2Y_3} = 10^{-6}\}$ and $\{(Y_3, Y_4, Y_5)\,|\,f_{Y_3Y_4Y_5} = 10^{-6}\}$. Because of the low value that these contours correspond to, most of the probability

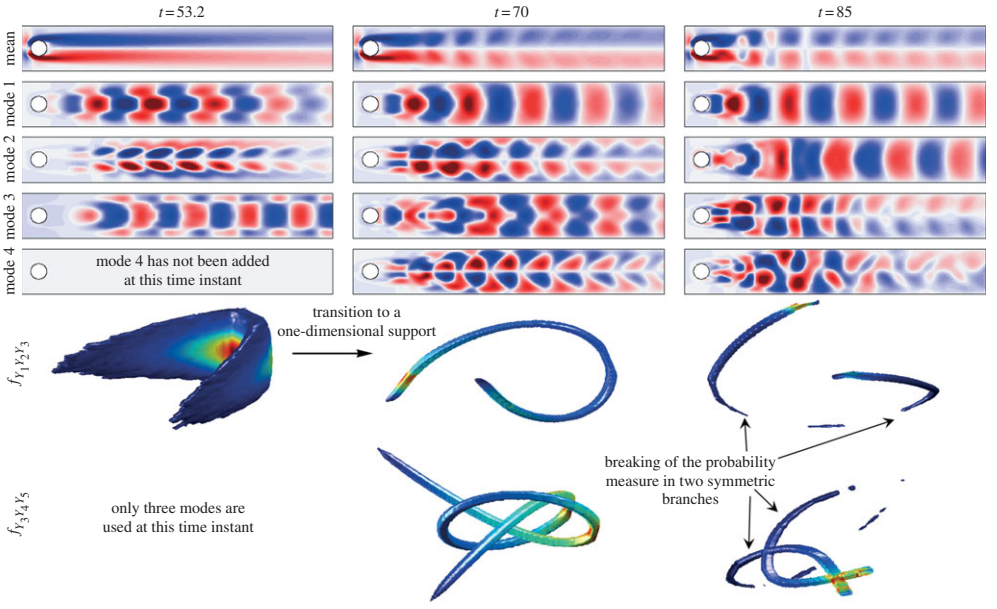

Figure 6. Stochastic flow behind a cylinder for $Re = 100$. In the upper plots, the vorticity fields for the mean flow and the first four DO modes (out of the eight used when the flow has been fully developed) are presented at times $t = 53, 70, 85$. In the lower plots, three-dimensional contours of the pdf are presented shaded according to the probability that is contained in the contour at each location (dark regions indicate lower probability). (Online version in colour.)

mass is contained inside these closed surfaces. Moreover, the colouring of the surfaces is according to the contained probability at each location of the contour (red regions corresponding to high probability and blue to low values).

At the second time instant ($t = 70$), we see that the probability measure has collapsed onto a one-dimensional curve with a shape that still expresses the symmetric features of the flow. Additionally, all of the modes have either symmetric or antisymmetric features. At this regime, essentially, every possible realization of the flow is a member of a one-dimensional family of solutions that 'live' on this manifold. The evolution of the probability measure continues ($t = 85$) with a breaking of the support into to two symmetric branches containing most of the probability. Despite this breaking, the dimensionality of these branches remain the same (one-dimensional) because there is no external noise applied to the reduced-order system that could cause an initial diffusion of the probability measure into directions that (by that time) have become unstable and which they need just an initial perturbation in order to lead to local dimensionality increase in the probability measure.

A detailed analysis of the energy transfer properties over the complete time interval is beyond the scope of this work and will be presented in Sapsis *et al*. [34]. Here, we want to illustrate the transition of the attractor from two-dimensional to one-dimensional. To this end, we will now focus on the dimensionality decrease right after the first presented time instant ($t = 53$). In figure 7, we show the probability measure (through the contour $\{(Y_1, Y_2, Y_3) \,|\, f_{Y_1Y_2Y_3} = 10^{-6}\}$) and the corresponding scatter plot associated with the reduced-order dynamics at two time instants $t = 54$ and $t = 56$. The contour is shaded (coloured in online version) according to the local number of positive FTLE (with integration time $\delta t = 1.6$) which expresses the number of finite-time instabilities at each location $(Y_1, Y_2, \ldots, Y_s)$ of the phase space. Specifically, the dark (blue in online version) regions that cover most of the probability measure correspond to locations with one positive FTLE, whereas the much smaller light (green in online version) regions correspond to locations of two positive FTLE. This is in accordance with theorem 2.1, which states that the local dimensionality of the support of the probability measure cannot exceed for sufficiently long time intervals the number of positive FTLE.

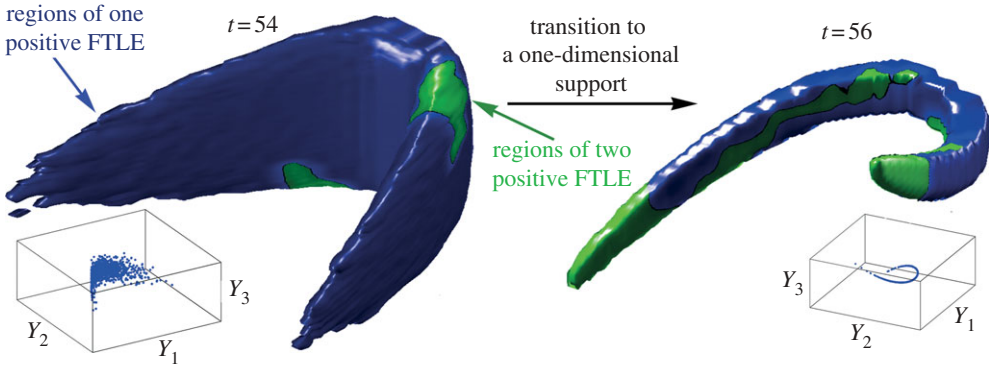

Figure 7. Three-dimensional contours of the probability density function $f_{Y_1Y_2Y_3}$ for two different time instants between which the dimensionality of the support of the pdf decreases. The shading is according to the number of positive FTLE: dark (blue in online version) indicates one positive FTLE and grey (green show in online version) two positive FTLE. The scatter plots for each density are also presented. (Online version in colour.)

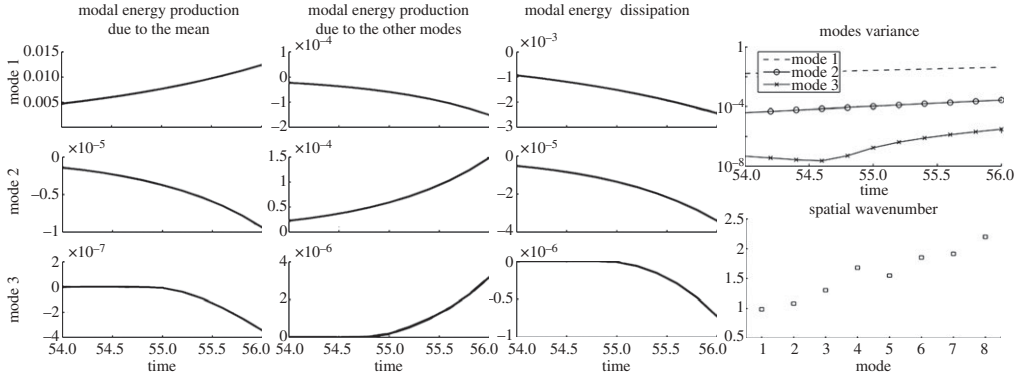

Figure 8. Flow behind a disc. (upper plots) Modal energy production (i) due to the mean flow (first column), (ii) due to the other DO modes (second column); modal energy dissipation (third column). Variance of the three first modes (top right); average spatial wavenumber for each DO mode (equation (5.2)) (bottom right).

For the same time interval, we examine the transfer of energy among different dynamical components by plotting (figure 8) the corresponding energy productions (equation (5.1)). We observe that consistently with the previous calculations of positive FTLE we have only the first mode absorbing energy from the mean flow. Subsequently, one part of this energy is dissipated, and the rest passes to the other two DO modes through the quadratic term in the reduced-order dynamics. This 'targeted energy transfer' has been previously observed in strongly nonlinear mechanical systems [36] and as it has been proved in this case it is due to the existence of a perturbed homoclinic orbit that governs the dynamics [37]. These two DO modes dissipate one part of this energy and the rest is returned back to the mean flow. We emphasize that the amount of energy dissipated has the same order of magnitude with the amount of energy that is transferred to or from the other DO modes. Note that this reverse flow of energy back to the mean flow is observed because we are having a fluid flow which is unstable but nevertheless laminar, i.e. the length scales of the high-order modes are large enough so that dissipation is small enough to be compared with the energy transfer back to the mean flow. In a turbulent regime, the length scales of the high-order modes would not permit an energy transfer back to the mean that is comparable to the dissipation.

In figure 8, we also present the average spatial wavenumber $\bar{k}$ for each DO mode, showing that in general higher modes contain energy in higher wavenumbers. Combining this result with

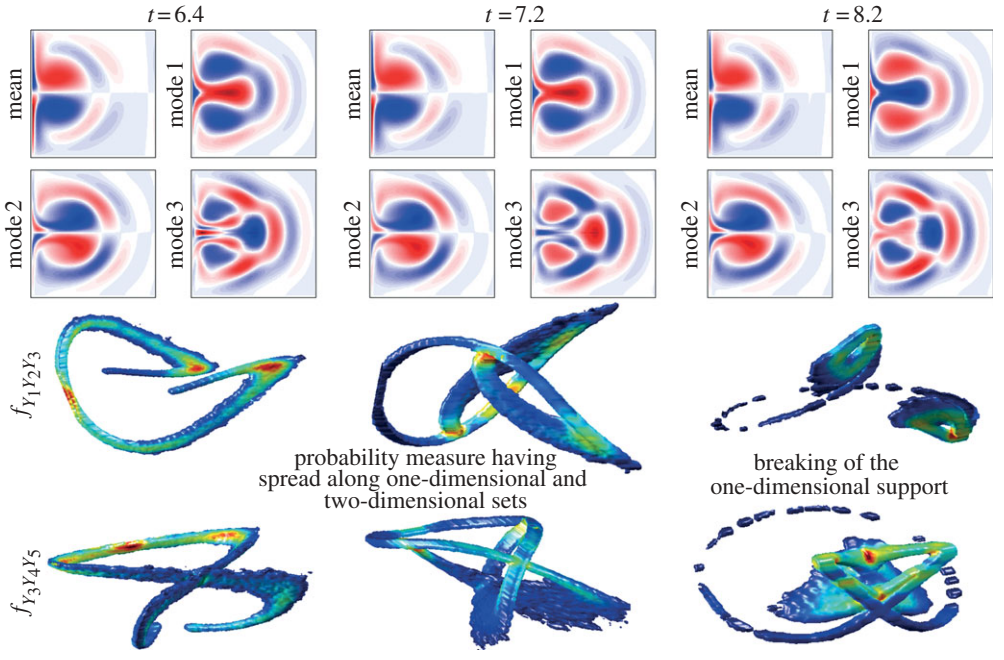

Figure 9. Wind-derived double gyre flow under deterministic forcing and with random initial conditions for $Re = 35$. In the upper plots, the vorticity fields for the mean flow, and the first three DO modes are presented at times $t = 6.4, 7.2, 8.2$. In the lower plots, three-dimensional contours of the pdf are presented shaded (coloured in online version) according to the probability that is contained in the contour at each location (dark regions indicate lower probability). (Online version in colour.)

the fact that only the first few modes absorb energy from the mean flow, then pass it to higher modes, which then return it to the mean flow again, we may conclude that the circulation of energy occurs from large length scales to smaller length scales and from there back to large length scales again. We have also seen how this circulation of energy between scales results in strongly non-Gaussian statistics that 'live' in very low dimensional objects. As we will see in §5*b*, these low dimensional objects are not necessarily manifolds because their dimensionality may not be uniform everywhere.

(b) Wind-driven double gyre flow

The next application that we consider is the wind-driven double gyre flow. The excitation is deterministic with no stochastic component and the Reynolds number is chosen $Re = 35$ (see Sapsis & Lermusiaux [38,39] for details on the system configuration). Contrary to the previous case that we examined, in this case, the DO modes reach a steady-state regime much earlier than the reduced-order stochastic dynamics that continue to evolve. Specifically, as we observe in figure 9, the shape of the modes remain invariant after the uncertainty associated with the modes has become important (see also the variance plot in figure 11).

During the same time interval, the probability measure undergoes through important transitions that involve both its shape and the dimensionality of its support. Specifically, as it can be seen in figure 9, the initially Gaussian probability measure rapidly collapses into a two-dimensional strip having very small width ($t = 5.4$). In the next time instant ($t = 7.2$), the probability measures 'lives' in a hybrid support that consists of both one- and two-dimensional domains. These two regions indicate the existence of two different kinds of instabilities that have different extend into the stochastic subspace. In some part of the subspace, they coexist giving rise to two-dimensional support for the probability measure, whereas in some other locations, only one of them persists resulting in a one-dimensional support for the probability measure. This

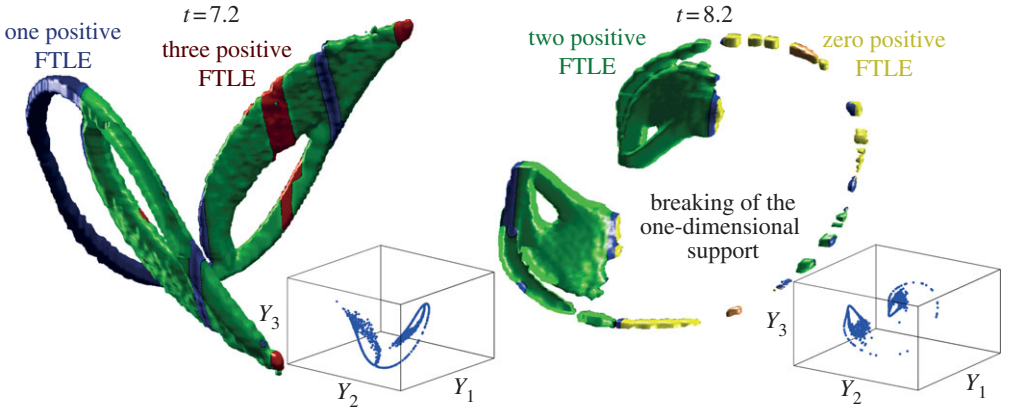

Figure 10. Three-dimensional contours of the probability density function $f_{Y_1Y_2Y_3}$ for two different time instants between which the one-dimensional part of the support is breaking. The shading is according to the number of positive FTLE: very bright (yellow in online versions) indicates zero positive FTLE, dark (blue in online version): one positive FTLE, light (green in online version) two positive FTLE, and grey (red in online version) regions: three positive FTLE. The scatter plots for each density are also presented. (Online version in colour.)

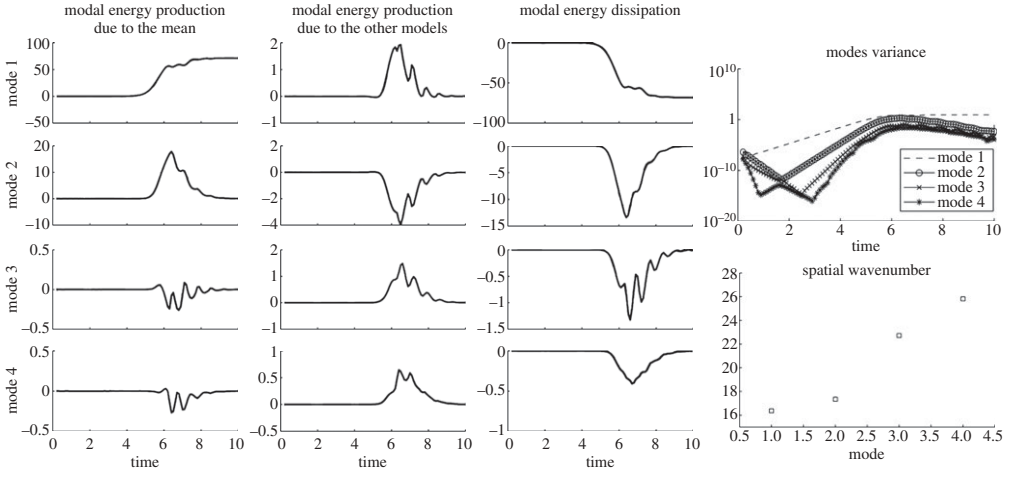

Figure 11. Double gyre flow. Modal energy production (i) due to the mean flow (first column), (ii) due to the other DO modes (second column); modal energy dissipation (third column); variance of the three four modes (top-right); average spatial wavenumber for each DO mode (equation (5.2)) (bottom-right).

hybrid form of the probability measure is not stable for a long time, because in a subsequent time instant ($t = 8.2$), the one-dimensional part of the support starts breaking into zero-dimensional points resulting in this way a symmetric, disconnected pair of two-dimensional sets.

The evolution of the form and dimensionality of the probability measure is in full consistency with the number of positive FTLE. These are shown as different colours over the contour of the probability density function in figure 10. We observe that at time $t = 7.2$ we mainly have two kinds of domains: those with one positive FTLE (dark or blue in online version) and the ones with two positive FTLE (light or green in online version). The dimensionality of the attractor follows exactly these dynamical characteristics. In the latter time instant $t = 8.2$, we observe that the breaking of the one-dimensional part of the support is caused due to a dynamical transition that results in zero positive FTLE in this area of the phase space. In particular, we observe that the domain that was previously characterized by one positive FTLE and which was one-dimensional now has all the FTLE negative causing the probability measure to concentrate around individual points.

Finally, the dimensionality of the attractor can also be interpreted in terms of the energy transfer properties that are shown in figure 11. The first mode, which is unstable, acts almost independently from the rest as it absorbs energy from the mean flow and subsequently dissipates it almost completely. Its interaction with the other modes is restricted on the absorption of a very small amount of energy that mainly comes from the second mode. On the other hand, the other three modes present strong interactions. The second mode, which also absorbs energy from the mean, acts as source of energy for modes 3 and 4. These stable modes take part of this energy (through the quadratic terms in the reduced-order equations), dissipate one part of it, and then return the rest (which is comparable in magnitude to the part that is dissipated) to the mean flow. The average wavelength for each mode confirms that the circulation of energy occurs from large length scales to smaller ones and then back to larger length scales again. Similarly, with the previous example, this reverse flow of energy takes place because the flow is essentially laminar (even though unstable), and the length scales of the high-energy modes are still very large so that dissipation is comparable with the energy transfer to the mean.

6. Conclusions and future directions

We have established a direct link between the local geometrical properties of the attractor and the number of instabilities for deterministic systems having unstable directions. This connection was proved and illustrated through a probabilistic framework that allowed for the description of the attractor and the energy transfers more effectively. In particular, we have proved that the low local fractal dimensionality of the attractor is caused by the synergistic activity of stable and unstable modes (corresponding to negative and positive Lyapounov exponents) that cause contraction and expansion of volumes in the reduced-order phase space. We have also illustrated the important role of the quadratic terms in the reduced-order dynamics, which transfer energy from the unstable to the stable modes, keeping in this way, the energy of the former to bounded levels and the energy of the latter to non-zero levels.

Our theoretical findings have been numerically demonstrated and validated in specific applications involving two-dimensional fluid flows having a small number of instabilities. The stochastic order-reduction framework that we applied is the one based on the DO field equations. In contrast to the POD-based methodologies, the DO method allowed for the computation of the appropriate modes based on the current statistical state and the equations describing the system without requiring the usage of any empirical data in order to obtain information for the transient character of the dynamics.

Future research includes the use of the presented results and ideas towards the development of predictive capacity and understanding of the statistics of turbulent systems in high *Re* regimes where the large number of positive Lyapunov exponents (i.e. instabilities) leads to significant complexity (see Majda [40,41] for an overview of challenges and research directions in such problems). The large intrinsic dimensionality of these systems makes the direct application of order-reduction techniques, as those described here, a computationally challenging (and until now unresolved) problem and therefore, it is essential these order-reduction ideas to be combined with appropriate second-order schemes that can capture a larger part of the energy spectrum inexpensively. Results along this direction of blended methods will be reported in Sapsis & Majda [42,43].

The author thanks the anonymous reviewers for comments and suggestions that led to significant improvements of the manuscript. He is also grateful to Prof. Andrew Majda and Prof. Alexander Vakakis for stimulating discussions.

References

1. Hopf E. 1948 A mathematical example displaying features of turbulence. *Comm. Pure Appl. Math.* **1**, 303–322. (doi:10.1002/cpa.3160010401)

2. Foias C, Sell GR, Temam R. 1988 Inertial manifolds for nonlinear evolutionary equations. *J. Diff. Equ.* **73**, 309–353. (doi:10.1016/0022-0396(88)90110-6)
3. Foias C, Temam R. 1979 Some analytic and geometric properties of the solutions of the Navier–Stokes equations. *J. Math. Pure Appl.* **58**, 339.
4. Foias C, Nicolaenko B, Sell GR, Temam R. 1985 Inertial manifold for the Kuramoto–Shivashinsky equation. *C. R. Acad. Sci. I Math* **301**, 285.
5. Temam R. 1988 *Infinite-dimensional dynamical systems in mechanics and physics*. Berlin, Germany: Springer.
6. Foias C, Titi ES. 1991 Determining nodes, finite difference schemes and inertial manifolds. *Nonlinearity* **4**, 135. (doi:10.1088/0951-7715/4/1/009)
7. Foias C, Temam R. 1984 Determination of the solutions of Navier–Stokes equations by a set of nodal values. *Math. Comput.* **43**, 117–133. (doi:10.1090/S0025-5718-1984-0744927-9)
8. Foias C, Temam R. 1988 The algebraic approximation of attractors: the finite dimensional case. *Physica D* **32**, 163–182. (doi:10.1016/0167-2789(88)90049-8)
9. Foias C, Sell GT, Titi ES. 1989 Exponential tracking and approximation of inertial manifolds for dissipative nonlinear equations. *J. Dyn. Differ. Equ.* **1**, 199–244. (doi:10.1007/BF01047831)
10. Titi ES. 1990 On approximate inertial manifolds to the Navier–Stokes equations. *J. Math. Anal. Appl.* **149**, 540–557. (doi:10.1016/0022-247X(90)90061-J)
11. Aubry N, Holmes P, Lumley J, Stone E. 1988 The dynamics of coherent structures in the wall region of turbulent boundary layer. *J. Fluid Mech.* **192**, 115–173. (doi:10.1017/S0022112088001818)
12. Holmes P, Lumley J, Berkooz G. 1996 *Turbulence, coherent structures, dynamical systems and symmetry*. Cambridge, UK: Cambridge University Press.
13. Lall S, Marsden JE, Glavaski S. 2002 A subspace approach to balanced truncation for model reduction of nonlinear control systems. *Int. J. Robust Nonlinear Control* **12**, 519–535. (doi:10.1002/rnc.657)
14. Ma Z, Rowley CW, Tadmor G. 2010 Snapshot-based balanced truncation for linear time-periodic systems. *IEEE Trans. Autom. Control* **55**, 469–473. (doi:10.1109/TAC.2009.2036335)
15. Rowley CW, Mezic I, Bagheri S, Schlatter P, Henningson DS. 2009 Spectral analysis of nonlinear flows. *J. Fluid Mech.* **641**, 115–127. (doi:10.1017/S0022112009992059)
16. Noack BR, Afanasiev K, Morzynski M, Tadmor G, Thiele F. 2003 A hierarchy of low-dimensional models for the transient and post-transient cylinder wake. *J. Fluid Mech.* **497**, 335–363. (doi:10.1017/S0022112003006694)
17. Tadmor G, Lehmann O, Noack BR, Morzynski M. 2010 Mean field representation of the natural and actuated cylinder wake flow. *Phys. Fluids* **22**, 034102. (doi:10.1063/1.3298960)
18. Tadmor G, Lehmann O, Noack BR, Cordier L, Delville J, Bonnet JP, Morzynski M. 2011 Reduced order models for closed-loop wake control. *Phil. Trans. R. Soc. A* **369**, 1513–1524. (doi:10.1098/rsta.2010.0367)
19. Sapsis TP. Lermusiaux PFJ. 2009 Dynamically orthogonal field equations for continuous stochastic dynamical systems. *Physica D* **238**, 2347–2360. (doi:10.1016/j.physd.2009.09.017)
20. Rempfer D, Fasel HF. 1994 Dynamics of three-dimensional coherent structures in a flat-plate boundary layer. *J. Fluid Mech.* **275**, 257–283. (doi:10.1017/S0022112094002351)
21. Sapsis TP. 2010 *Dynamically orthogonal field equations for stochastic fluid flows and particle dynamics*. PhD Thesis, MIT, Cambridge, MA.
22. Rozanov YA. 1996 *Random fields and stochastic partial differential equations*. Amsterdam, the Netherlands: Kluwer Academic Publishers.
23. Sobczyk K. 1985 *Stochastic wave propagation*. Amsterdam, The Netherlands, Elsevier.
24. Haller G. 2011 A variational theory of hyperbolic lagrangian coherent structures. *Physica D* **240**, 574–598. (doi:10.1016/j.physd.2010.11.010)
25. Sobczyk K. 1991 *Stochastic differential equations*. Dordrecht, the Netherlands: Kluwer Academic Publishers.
26. Sapsis TP, Athanassoulis GA. 2008 New partial differential equations governing the joint, response–excitation, probability distributions of nonlinear systems, under general stochastic excitation. *Probab. Eng. Mech.* **23**, 289–306. (doi:10.1016/j.probengmech.2007.12.028)
27. Pesin YB. 1998 *Dimension theory in dynamical systems: contemporary views and applications*. Chicago, IL: University of Chicago.
28. Coddington E, Levinson N. 1955 *Theory of ordinary differential equations*. New York, NY: McGraw-Hill.

29. Young LS. 2002 What are SRB measures, and which dynamical systems have them? *J. Stat. Phys.* **108**, 733–754. (doi:10.1023/A:1019762724717)
30. Lorenz EN. 1963 Deterministic nonperiodic flow. *J. Atmos. Sci.* **20**, 130–141. (doi:10.1175/1520-0469(1963)020<0130:DNF>2.0.CO;2)
31. Grassberger P, Procaccia I. 1983 Measuring the strangeness of strange attractors. *Physica D* **9**, 189–208. (doi:10.1016/0167-2789(83)90298-1)
32. Haller G. 2001 Distinguished material surfaces and coherent structures in 3D fluid flows. *Physica D* **149**, 248–277. (doi:10.1016/S0167-2789(00)00199-8)
33. Lekien F, Shadden S, Marsden J. 2007 Lagrangian coherent structures in n-dimensional systems. *J. Math. Phys.* **48**, 1–19. (doi:10.1063/1.2740025)
34. Sapsis TP, Ueckermann MP. Lermusiaux PFJ. Submitted. Global analysis of Navier–Stokes and boussinesq stochastic flows using dynamical orthogonality.
35. Ueckermann MP. Lermusiaux PFJ. Sapsis TP. 2013 Numerical schemes for dynamically orthogonal equations of stochastic fluid and ocean flows. *J. Comput. Phys.* **233**, 272–294. (doi:10.1016/j.jcp.2012.08.041)
36. Vakakis AF, Gendelman OV, Bergman LA, McFarland DM, Kerschen G, Lee YS. 2008 *Nonlinear targeted energy transfer in mechanical and structural systems*. Berlin, Germany: Springer.
37. Sapsis TP, Vakakis AF, Gendelman OV, Bergman LA, Kerschen G, Quinn DD. 2009 Efficiency of targeted energy transfer in coupled oscillators associated with 1:1 resonance captures. II. Analytical study. *J. Sound Vib.* **325**, 297–320. (doi:10.1016/j.jsv.2009.03.004)
38. Sapsis TP, Lermusiaux PFJ. 2012 Dynamical criteria for the evolution of the stochastic dimensionality in flows with uncertainty. *Physica D* **241**, 60–76. (doi:10.1016/j.physd.2011.10.001)
39. Sapsis TP, Dijkstra HA. In press Interaction of external stochastic excitation and nonlinear dynamics in wind-driven ocean circulation flows. *J. Phys. Oceanogr.*
40. Majda AJ. 2000 Real world turbulence and modern applied mathematics. In *Mathematics: frontiers and perspectives, International Mathematical Union* (eds VI Arnold, M Atiyah, P Lax, B Mazur), pp. 137–151. Providence, MA: American Mathematical Society.
41. Majda AJ. 2012 Challenges in climate science and contemporary applied mathematics. *Commun. Pure Appl. Math.* **65**, 920–948. (doi:10.1002/cpa.21401)
42. Sapsis TP, Majda AJ. In press. A statistically accurate modified quasilinear gaussian closure for uncertainty quantification in turbulent dynamical systems. *Physica D*. (doi:10.1016/j.physd.2013.02.009)
43. Sapsis TP, Majda AJ. Submitted. Blended reduced subspace algorithms for uncertainty quantification of quadratic systems with a stable mean state.

Attractor local dimensionality, nonlinear energy transfers, and finite-time instabilities in unstable dynamical systems with applications to 2D fluid flows

Themistoklis P. Sapsis
Massachusetts Institute of Technology, Department of Mechanical Engineering
77 Massachusetts Av., Cambridge, MA 02139, USA

Appendix S1 - Comparison of DO with POD

Here we will perform a comparison of the DO and POD method as order-reduction techniques. Since, the DO method produces a set of time-dependent modes it is natural to expect that it will be more efficient on representing the transient dynamics observed in complex systems, such as fluid flows, compared with the POD method that uses a static set of modes. Moreover, because the computation of the DO modes is based on a set of equations that follows directly from the original system equation, no numerical or experimental series of runs is required, in contrary to the POD method. However, it must be pointed out that the numerical implementation of the DO method is more complicated than a deterministic PDE solver although the computational cost associated with the former method is significantly smaller compared with the generation of a large set of numerical realizations which are necessary in order to apply the POD method.

We consider the flow behind a cylinder for $\mathrm{Re}=100$ presented in Sapsis & Lermusiaux (2009) as well as the double gyre flow in a basin (Simmonet & Dijkstra (2002)) in the presence of external excitation studied in detail in Sapsis & Dijkstra (2013) for $\mathrm{Re}=50$. The specific details for resolving Navier-Stokes equations in the framework of DO equations (treatment of stochastic pressure, boundary conditions, etc.) can be found in Sapsis (2010) and Sapsis *et al.* (2013) while the description of the numerical scheme used in this paper is given in Ueckermann *et al.* (2013). After obtaining the stochastic solution we compute the number of required POD modes to represent the mean field and each time-dependent DO mode using the method of snapshots (Sirovich (1987)). Specifically, we consider the mean field and the DO modes on m time instants, $t_1,...,t_m$. We first compute the temporal average for the mean flow and the weighted temporal average for the modes (weighted with respect to the typical deviation $\sigma_i(t_k)=\sqrt{E^\omega\left[Y_i^2(t_k;\omega)\right]}$ since each DO mode is spatially orthonormal and does not carry temporal energy information but only how energy is distributed in space)

$$A[\bar{u}](x)=\frac{1}{m}\sum_{k=1}^{m}\bar{u}(x,t_k),\quad A[u_i](x)=\frac{1}{m}\sum_{k=1}^{m}\sigma_i(t_k)\,u_i(x,t_k),\quad i=1,...,s.$$

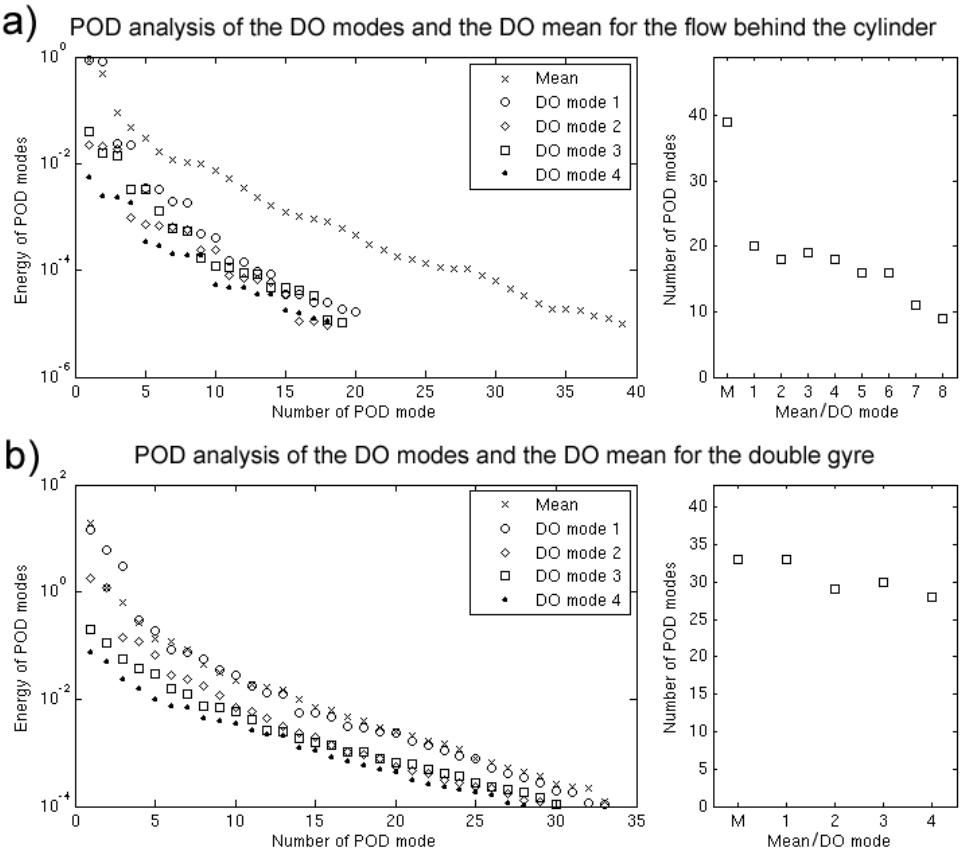

Figure 1. POD analysis of the DO modes and the DO mean for a) the flow behind the cylinder and b) the double gyre flow. Left column: Energy of the POD modes which are necessary to represent the mean flow and the first four DO modes; Right column: Number of (static) POD modes necessary to represent the (time-dependent) mean flow and each (time-dependent) DO mode.

Then we compute the matrices

$$\mathbf{R}_{mean} = \frac{1}{m}\int_D \left(\bar{u}\left(x,t_k\right) - A\left[\bar{u}\right]\left(x\right)\right)^T \left(\bar{u}\left(x,t_l\right) - A\left[\bar{u}\right]\left(x\right)\right) dx \in \mathbb{R}^{m\times m},$$

$$\mathbf{R}_{DO,i} = \frac{1}{m}\int_D \left(\sigma_i\left(t_k\right) u_i\left(x,t_k\right) - A\left[u_i\right]\left(x\right)\right)^T \left(\sigma_i\left(t_l\right) u_i\left(x,t_l\right) - A\left[u_i\right]\left(x\right)\right) dx \in \mathbb{R}^{m\times m},$$

for all $i = 1, ..., s$. By diagonalizing these matrices we obtain the energy of the corresponding POD modes as the eigenvalues of the diagonalization problem. We keep only the eigenvalues (and the corresponding POD modes) having energy larger than $\rho = \max_{t,i}\left[E^{\omega}\left[Y_i^2\left(t;\omega\right)\right]\right]$ where ρ is a very small parameter chosen to be $\rho = 10^{-6}$.

The first example that we consider is the flow behind the cylinder for $\mathrm{Re}=100$. The flow is initiated with a small stochastic perturbation which grows rapidly due to internal instabilities of the flow. The number of DO modes that we use is adaptive (Sapsis & Lermusiaux (2012)) with maximum number of modes $s=8$. In Figure 1a the comparison with the POD method is illustrated. Specifically, in the left panel we observe the energy of the POD modes required to represent adequately the mean field and each of the DO modes. It is interesting to note that each DO mode contains a large number (order 10-100) of POD modes (the exact number for each DO mode and the mean is shown in the lower-right panel) as it was expected from the beginning since the DO modes are time-dependent fields. It is also clear that each DO mode contains both high and low energy POD modes a property that illustrates the nature of the DO modes as a time-dependent reduced-order basis that comes directly from the system equations and not from energy based criteria as it is the case with the POD modes. Finally, an interesting point involves the mean flow as this is computed from the DO equations which requires the largest number of POD modes to be represented (compared with the DO modes) illustrating clearly the importance of the mean flow variations as an intrinsic component of the transient character of the response (Tadmor *et al.* (2010), Tadmor *et al.* (2011)).

In Figure 1b we present the corresponding results for the double gyre flow (see Sapsis & Dijkstra (2013) for details). This stochastic flow is resolved with a fixed number of modes ($s=4$). Similarly with the previous example, here we also have a large number of POD modes associated with each DO mode and the mean field illustrating the strongly transient character of the dynamics involved. Contrary to the previous case we observe that the mean field requires comparable number of modes with the DO modes in order to be represented adequately.

From the last two cases it is clear that a time-dependent basis generated from the DO equations is more efficient than even a large number of static POD modes. Specifically, using the DO order-reduction approach we are able to describe the mean field temporal variations as well as the time-dependent modes which contain a large series of POD modes ranging from high energy, large scale elements to lower energy components with small spatial wavelengths. These time-dependent modes are particularly efficient in capturing the strongly transient, low-dimensional, dynamics observed in the flows considered in this work.

Appendix S2 - Proof of Lemma 1

We consider Gauss identity: $\int_D \frac{\partial a}{\partial x_j} F_j d\mathbf{x} = -\int_D a \frac{\partial F_j}{\partial x_j} d\mathbf{x} + \int_{\partial D} a F_j n_j d\mathbf{s}$ which holds for any sufficiently smooth scalar field a and vector field F_j. We apply the above identity for $F_j = \beta \Phi_j$ where Φ_j is a divergence-free field and β is a smooth scalar field. We then obtain

$$\int_D \frac{\partial a}{\partial x_j} \beta \Phi_j d\mathbf{x} = -\int_D a \frac{\partial \beta}{\partial x_j} \Phi_j dx + \int_{\partial D} a \beta \Phi_j n_j d\mathbf{s}.$$

Using this identity we will have

$$\langle \mathbf{u}_n.\nabla \mathbf{u}_m, \mathbf{u}_i \rangle = \int\limits_D \frac{\partial u_{m,k}}{\partial x_j} u_{n,j} u_{i,k} d\mathbf{x} = -\langle \mathbf{u}_n.\nabla \mathbf{u}_i, \mathbf{u}_m \rangle + \int\limits_{\partial D} u_{m,k} u_{i,k} u_{n,j} n_j ds. \tag{0.1}$$

Now, for any scalar, global, quantity $Q = \int\limits_D q(x,t)\, dx$ which is preserved in time, i.e. $\frac{dQ}{dt} = 0$ we will have

$$0 = \int\limits_D \frac{d}{dt} q(\mathbf{x},t)\, d\mathbf{x} = \int\limits_D \left(\frac{\partial q}{\partial t} + \frac{\partial q}{\partial x_j} u_j \right) d\mathbf{x} = \int\limits_D \frac{\partial q}{\partial t} d\mathbf{x} + \int\limits_{\partial D} q u_j n_j d\mathbf{s}.$$

We apply the above for $q = u_{m,k} u_{i,k}$. Obviously we have $\frac{dQ}{dt} = 0$ since orthonormality of modes is preserved by the DO equations. Moreover by direct application of the orthonormality condition we have

$$\int\limits_D \frac{\partial q}{\partial t} d\mathbf{x} = \int\limits_D \left(\frac{\partial u_{m,k}}{\partial t} u_{i,k} + \frac{\partial u_{i,k}}{\partial t} u_{m,k} \right) d\mathbf{x} = 0 \Rightarrow \int\limits_{\partial D} u_{m,k} u_{i,k} u_j n_j d\mathbf{s} = 0.$$

Now, $u_j = \bar{u}_j + Y_n u_{n,j}$. Thus,

$$\int\limits_{\partial D} u_{m,k} u_{i,k} \bar{u}_j n_j d\mathbf{s} + Y_n \int\limits_{\partial D} u_{m,k} u_{i,k} u_{n,j} n_j d\mathbf{s} = 0 \Leftrightarrow$$

$$\int\limits_{\partial D} u_{m,k} u_{i,k} \bar{u}_j n_j d\mathbf{s} = \int\limits_{\partial D} u_{m,k} u_{i,k} u_{n,j} n_j d\mathbf{s} = 0,$$

since the first equality holds for all $\omega \in \Omega$. From the last equation and the Gauss identity shown previously we obtain Lemma 1. □

References

Sapsis, T. P. 2010 *Dynamically orthogonal field equations for stochastic fluid flows and particle dynamics*. MIT, PhD Thesis.

Sapsis, T. P. & Dijkstra, H. 2013 Interaction of noise and nonlinear dynamics in the double-gyre wind-driven ocean circulation. *J. Phys. Oceanography (In Press)* .

Sapsis, T. P. & Lermusiaux, P. F. J. 2009 Dynamically orthogonal field equations for continuous stochastic dynamical systems. *Physica D* **238**, 2347–2360.

Sapsis, T. P. & Lermusiaux, P. F. J. 2012 Dynamical criteria for the evolution of the stochastic dimensionality in flows with uncertainty. *Physica D* **241**, 60.

Sapsis, T. P., Ueckermann, M. P. & Lermusiaux, P. F. J. 2013 Global analysis of navier-stokes and boussinesq stochastic flows using dynamical orthogonality. *J. Fluid. Mech. (Submitted)* .

Simmonet, E. & Dijkstra, H. 2002 Spontaneous generation of low-frequency modes of variability in the wind-driven ocean circulation. *J. Phys. Oceanography* **32**, 1747–1762.

Sirovich, L. 1987 Turbulence and the dynamics of coherent structures, parts I, II and III. *Quart. Appl. Math.* **XLV**, 561–590.

Tadmor, G., Lehmann, O., Noack, B. R., Cordier, L., Delville, J., Bonnet, J. P. & Morzynski, M. 2011 Reduced order models for closed-loop wake control. *Philosophical Trans. Royal Soc. A* **369**, 1513–1524.

Tadmor, G., Lehmann, O., Noack, B. R. & Morzynski, M. 2010 Mean field representation of the natural and actuated cylinder wake flow. *Phys. Fluids* **22**, 034102.

Ueckermann, M. P., Lermusiaux, P. F. J. & Sapsis, T. P. 2013 Numerical schemes for dynamically orthogonal equations of stochastic fluid and ocean flows. *J. Comput. Phys.* **233**, 272–294.